9 Hecht, J. T., Hogue, D., Wang, Y., Blanton, S. H., Wagner, M., Strong, L. C., Raskind, W., Hansen, M. F. and Wells, D. (1997) Hereditary multiple exostoses (EXT): mutational studies of familial EXT1 cases and EXT-associated malignancies. Am. J. Hum. Genet. **60**, 80–86

10 Senay, C., Lind, T., Muguruma, K., Tone, Y., Kitagawa, H., Sugahara, K., Lidholt, K., Lindahl, U. and Kusche-Gullberg, M. (2000) The EXT1/EXT2 tumor suppressors: catalytic activities and role in heparan sulfate biosynthesis. EMBO Rep. **1**, 282–286

11 McCormick, C., Duncan, G., Goutsos, K. T. and Tufaro, F. (2000) The putative tumor suppressors EXT1 and EXT2 form a stable complex that accumulates in the Golgi apparatus and catalyzes the synthesis of heparan sulfate. Proc. Natl. Acad. Sci. U.S.A. **97**, 668–673

12 Van Hul, W., Balemans, W., Van Hul, E., Dikkers, F. G., Obee, H., Stokroos, R. J., Hildering, P., Vanhoenacker, F., Van Camp, G. and Willems, P. J. (1998) Van Buchem disease (hyperostosis corticalis generalisata) maps to chromosome 17q12-q21. Am. J. Hum. Genet. **62**, 391–399

13 Wise, C. A., Clines, G. A., Massa, H., Trask, B. J. and Lovett, M. (1997) Identification and localization of the gene for EXTL, a third member of the multiple exostoses gene family. Genome Res. **7**, 10–16

14 Wuyts, W., Van Hul, W., Hendrickx, J., Speleman, F., Wauters, J., De Boulle, K., Van Roy, N., Van Agtmael, T., Bossuyt, P. and Willems, P. J. (1997) Identification and characterization of a novel member of the EXT gene family, EXTL2. Eur. J. Hum. Genet. **5**, 382–389

15 Saito, T., Seki, N., Yamauchi, M., Tsuji, S., Hayashi, A., Kozuma, S. and Hori, T. (1998) Structure, chromosomal location, and expression profile of EXTR1 and EXTR2, new members of the multiple exostoses gene family. Biochem. Biophys. Res. Commun. **243**, 61–66

16 Kim, B. T., Kitagawa, H., Tamura, J., Saito, T., Kusche-Gullberg, M., Lindahl, U. and Sugahara, K. (2001) Human tumor suppressor EXT gene family members EXTL1 and EXTL3 encode α1,4-N-acetylglucosaminyltransferases that likely are involved in heparan sulfate/heparin biosynthesis. Proc. Natl. Acad. Sci. U.S.A. **98**, 7176–7181

17 Kim, B. T., Kitagawa, H., Tanaka, J., Tamura, J. and Sugahara, K. (2003) *In vitro* heparan sulfate polymerization: crucial roles of core protein moieties of primer substrates in addition to the EXT1–EXT2 interaction. J. Biol. Chem. **278**, 41618–41623

18 Kitagawa, H., Kano, Y., Shimakawa, H., Goto, F., Ogawa, T., Okabe, H. and Sugahara, K. (1999) Identification and characterization of a novel UDP-GalNAc:GlcAβ-R α1,4-N-acetylgalactosaminyltransferase from a human sarcoma cell line. Glycobiology **9**, 697–703

19 Kitagawa, H., Shimakawa, H. and Sugahara, K. (1999) The tumor suppressor EXT-like gene EXTL2 encodes an α1, 4-N-acetylhexosaminyltransferase that transfers N-acetylgalactosamine and N-acetylglucosamine to the common glycosaminoglycan-protein linkage region: the key enzyme for the chain initiation of heparan sulfate. J. Biol. Chem. **274**, 13933–13937

20 Pedersen, L. C., Dong, J., Taniguchi, F., Kitagawa, H., Krahn, J. M., Pedersen, L. G., Sugahara, K. and Negishi, M. (2003) Crystal structure of an α1,4-N-acetylhexosaminyltransferase (EXTL2), a member of the exostosin gene family involved in heparan sulfate biosynthesis. J. Biol. Chem. **278**, 14420–14428

21 Lin, X., Wei, G., Shi, Z., Dryer, L., Esko, J. D., Wells, D. E. and Matzuk, M. M. (2000) Disruption of gastrulation and heparan sulfate biosynthesis in EXT1-deficient mice. Dev. Biol. **224**, 299–311

22 Toyoda, H., Kinoshita-Toyoda, A., Fox, B. and Selleck, S. B. (2000) Structural analysis of glycosaminoglycans in animals bearing mutations in sugarless, sulfateless, and tout-velu: *Drosophila* homologues of vertebrate genes encoding glycosaminoglycan biosynthetic enzymes. J. Biol. Chem. **275**, 21856–21861

23 Kitagawa, H., Kinoshita, A. and Sugahara, K. (1995) Microanalysis of glycosaminoglycan-derived disaccharides labeled with the fluorophore 2-aminoacridone by capillary electrophoresis and high-performance liquid chromatography. Anal. Biochem. **232**, 114–121

24 McCormick, C., Leduc, Y., Martindale, D., Mattison, K., Esford, L. E., Dyer, A. P. and Tufaro, F. (1998) The putative tumour suppressor EXT1 alters the expression of cell-surface heparan sulfate. Nat. Genet. **19**, 158–161

25 Busse, M., Feta, A., Presto, J., Wilen, M., Gronning, M., Kjellen, L. and Kusche-Gullberg, M. (2007) Contribution of EXT1, EXT2, and EXTL3 to heparan sulfate chain elongation. J. Biol. Chem. **282**, 32802–32810

26 Yamada, S., Busse, M., Ueno, M., Kelly, O. G., Skarnes, W. C., Sugahara, K. and Kusche-Gullberg, M. (2004) Embryonic fibroblasts with a gene trap mutation in Ext1 produce short heparan sulfate chains. J. Biol. Chem. **279**, 32134–32141

27 Ropero, S., Setien, F., Espada, J., Fraga, M. F., Herranz, M., Asp, J., Benassi, M. S., Franchi, A., Patino, A., Ward, L. S. et al. (2004) Epigenetic loss of the familial tumor-suppressor gene exostosin-1 (EXT1) disrupts heparan sulfate synthesis in cancer cells. Hum. Mol. Genet. **13**, 2753–2765

28 Giulian, D., Haverkamp, L. J., Yu, J., Karshin, W., Tom, D., Li, J., Kazanskaia, A., Kirkpatrick, J. and Roher, A. E. (1998) The HHQK domain of β-amyloid provides a structural basis for the immunopathology of Alzheimer's disease. J. Biol. Chem. **273**, 29719–29726

29 Karibe, T., Fukui, H., Sekikawa, A., Shiratori, K. and Fujimori, T. (2008) EXTL3 promoter methylation down-regulates EXTL3 and heparan sulphate expression in mucinous colorectal cancers. J. Pathol. **216**, 32–42

30 Han, C., Belenkaya, T. Y., Khodoun, M., Tauchi, M., Lin, X. and Lin, X. (2004) Distinct and collaborative roles of *Drosophila* EXT family proteins in morphogen signalling and gradient formation. Development **131**, 1563–1575

31 Busse, M. and Kusche-Gullberg, M. (2003) *In vitro* polymerization of heparan sulfate backbone by the EXT proteins. J. Biol. Chem. **278**, 41333–41337

32 Stickens, D., Zak, B. M., Rougier, N., Esko, J. D. and Werb, Z. (2005) Mice deficient in Ext2 lack heparan sulfate and develop exostoses. Development **132**, 5055–5068

33 Nadanaka, S., Ishida, M., Ikegami, M. and Kitagawa, H. (2008) Chondroitin 4-O-sulfotransferase-1 modulates Wnt-3a signaling through control of E disaccharide expression of chondroitin sulfate. J. Biol. Chem. **283**, 27333–27343

34 Takahashi, I., Noguchi, N., Nata, K., Yamada, S., Kaneiwa, T., Mizumoto, S., Ikeda, T., Sugihara, K., Asano, M., Yoshikawa, T et al. (2009) Important role of heparan sulfate in postnatal islet growth and insulin secretion. Biochem. Biophys. Res. Commun. **383**, 113–118

35 Bornemann, D. J., Duncan, J. E., Staatz, W., Selleck, S. and Warrior, R. (2004) Abrogation of heparan sulfate synthesis in *Drosophila* disrupts the Wingless, Hedgehog and Decapentaplegic signaling pathways. Development **131**, 1927–1938

36 Takei, Y., Ozawa, Y., Sato, M., Watanabe, A. and Tabata, T. (2004) Three *Drosophila* EXT genes shape morphogen gradients through synthesis of heparan sulfate proteoglycans. Development **131**, 73–82

37 Izumikawa, T., Egusa, N., Taniguchi, F., Sugahara, K. and Kitagawa, H. (2006) Heparan sulfate polymerization in *Drosophila*. J. Biol. Chem. **281**, 1929–1934

38 Kim, B. T., Kitagawa, H., Tamura, J., Kusche-Gullberg, M., Lindahl, U. and Sugahara, K. (2002) Demonstration of a novel gene *DEXT3* of *Drosophila melanogaster* as the essential *N*-acetylglucosamine transferase in the heparan sulfate biosynthesis: chain initiation and elongation. J. Biol. Chem. **277**, 13659–13665

39 Kitagawa, H., Izumikawa, T., Mizuguchi, S., Dejima, K., Nomura, K. H., Egusa, N., Taniguchi, F., Tamura, J., Gengyo-Ando, K., Mitani, S. et al. (2007) Expression of rib-1, a *Caenorhabditis elegans* homolog of the human tumor suppressor EXT genes, is indispensable for heparan sulfate synthesis and embryonic morphogenesis. J. Biol. Chem. **282**, 8533–8544

40 Lee, J. S., von der Hardt, S., Rusch, M. A., Stringer, S. E., Stickney, H. L., Talbot, W. S., Geisler, R., Nusslein-Volhard, C., Selleck, S. B., Chien, C. B. and Roehl, H. (2004) Axon sorting in the optic tract requires HSPG synthesis by ext2 (dackel) and ext13 (boxer). Neuron **44**, 947–960

41 Esko, J. D. and Selleck, S. B. (2002) Order out of chaos: assembly of ligand binding sites in heparan sulfate. Annu. Rev. Biochem. **71**, 435–471

42 Presto, J., Thuveson, M., Carlsson, P., Busse, M., Wilen, M., Eriksson, I., Kusche-Gullberg, M. and Kjellen, L. (2008) Heparan sulfate biosynthesis enzymes EXT1 and EXT2 affect NDST1 expression and heparan sulfate sulfation. Proc. Natl. Acad. Sci. U.S.A. **105**, 4751–4756

43 Merry, C. L., Bullock, S. L., Swan, D. C., Backen, A. C., Lyon, M., Beddington, R. S., Wilson, V. A. and Gallagher, J. T. (2001) The molecular phenotype of heparan sulfate in the Hs2st$^{-/-}$ mutant mouse. J. Biol. Chem. **276**, 35429–35434

44 Uhlin-Hansen, L., Kusche-Gullberg, M., Berg, E., Eriksson, I. and Kjellen, L. (1997) Mouse mastocytoma cells synthesize undersulfated heparin and chondroitin sulfate in the presence of brefeldin A. J. Biol. Chem. **272**, 3200–3206

45 Gopal, S., Bober, A., Whiteford, J. R., Multhaupt, H. A., Yoneda, A. and Couchman, J. R. (2010) Heparan sulfate chain valency controls syndecan-4 function in cell adhesion. J. Biol. Chem, doi:jbc.M109.056945

46 Liuzzo, J. P. and Moscatelli, D. (1996) Human leukaemia cell lines bind basic fibroblast growth factor (FGF) on FGF receptors and heparan sulfates: downmodulation of FGF receptors by phorbol ester. Blood **87**, 245–255

Received 15 January 2010/24 March 2010; accepted 9 April 2010
Published as BJ Immediate Publication 9 April 2010, doi:10.1042/BJ20100101

Biochem. J. (2010) **428**, 463–471 (Printed in Great Britain) doi:10.1042/BJ20100101

online data

SUPPLEMENTARY ONLINE DATA
Biosynthesis of heparan sulfate in *EXT1*-deficient cells

Megumi OKADA*[1], Satomi NADANAKA*[1], Naoko SHOJI*[1], Jun-ichi TAMURA† and Hiroshi KITAGAWA*[2]

*Department of Biochemistry, Kobe Pharmaceutical University, Kobe 658–8558, Japan, and †Department of Regional Environment, Faculty of Regional Sciences, Tottori University, Japan

Table S1 Primers used for qRT-PCR

h, human; m, mouse.

Target	5′-primer (5′→3′)	3′-primer(5′→3′)	Product length (bp)
hEXT1	CAGATTCCTGGAGGCTTT	ATCCTGATGAATAGACCTGATTGT	164
hEXT2	TCCAAGGTGCCCAGTCTA	AGAACAGCTTCTGTCTCGAT	176
hEXTL1	GCCATCGTAGCTGATGAGAG	CAGAGTGGTATGGATGACCTT	150
hEXTL2	AGATGATACTCAAAACTGTGATGA	CAATAAGACCTCTGCAGAGC	176
hEXTL3	GGTTCACTCTTTCAAGAAGTCG	AGTGTCTATTCACAGTTATACAGTAATAGG	161
hGAPDH	ATGGGTGTGAACCATGAGAAGTA	GGCAGTGATGGCATGGAC	153
mEXT1	GGAGTTGCCATTCTCCGA	TAAGCCTCCCACAAGAACTG	153
mEXT2	AGTGTTAGTCTTGGACAAATGC	GCCAGCCTGTAGGACATC	178
mEXTL1	GGAGAGACCCTTCCCAATG	CTTGGTCCAGTCGATGACTT	153
mEXTL2	AACCGACTCCAGGTCTT	AACTGTAGATCCCGGAGG	178
mEXTL3	TACATCAACTGTGAGGATATCGC	ATAGCCGTACACCTTGACAAA	186
mGAPDH	CATCTGAGGGCCCACTG	GAGGCCATGTAGGCCATGA	205

Table S2 Disaccharide composition of HS from L, gro2C, gro2C-shEXT2, and gro2C-shEXTL2 and gro2C-shEXTL3 cells

Two different clones (clones 1 and 2) were established using two distinct shRNAs designed against each target gene and were then analysed. Values are expressed as pmol of disaccharide per mg of dried homogenate of these cells, and are means ± S.E.M. for three determinations. gro2C is an antibiotic-resistant clone selected by antibiotics after transfection with a empty vector (pLKO.1-Puro); ND, not detected; ΔDiHS-0S, ΔHexAα1-4GlcNAc; ΔDiHS-6S, ΔHexAα1-4GlcNAc(6S); ΔDiHS-NS, ΔHexAα1-4GlcNS; ΔDiHS-diS$_1$, ΔHexAα1-4Glc(NS,6S); ΔDi-diS$_2$, ΔHexA(2S)α1-4GlcNS; ΔDi-triS, ΔHexA(2S)α1-4Glc(NS,6S); HexA is hexuronic acid and NS is N-sulfated. Numbers in parentheses represent the percentage (mol/mol) of the total disaccharide content.

Disaccharide	L	gro2C	gro2C-shEXT2 clone 1	gro2C-shEXT2 clone 2	gro2C-shEXTL2 clone 1	gro2C-shEXTL2 clone 2	gro2C-shEXTL3 clone 1	gro2C-shEXTL3 clone 2
ΔDiHS-0S	617.5 ± 75.7 (37.4)	31.1 ± 4.0 (22.1)	12.3 ± 7.2 (32.1)	6.6 ± 2.6 (18.6)	15.7 ± 3.9 (29.4)	22.9 ± 1.2 (35.7)	48.9 ± 14.5 (35.1)	32.3 ± 0.9 (26.0)
ΔDiHS-6S	32.5 ± 10.3 (2.0)	10.4 ± 4.3 (7.3)	ND	0.3 ± 0.6 (0.9)	ND	ND	0.2 ± 0.3 (0.1)	0.5 ± 0.4 (0.4)
ΔDiHS-NS	555.1 ± 53.3 (33.6)	88.0 ± 8.1 (63.0)	25.4 ± 14.7 (66.3)	24.4 ± 4.3 (68.7)	35.3 ± 11.2 (65.8)	39.2 ± 13.5 (61.2)	89.2 ± 2.9 (64.0)	83.8 ± 8.8 (67.5)
ΔDiHS-diS[1]	30.3 ± 11.1 (1.8)	0.8 ± 1.3 (0.5)	ND	ND	ND	ND	ND	6.0 ± 0.2 (4.8)
ΔDiHS-diS[2]	273.9 ± 15.9 (16.6)	9.0 ± 1.3 (6.4)	ND	ND	1.4 ± 2.5 (2.7)	ND	1.1 ± 0.5 (0.8)	0.8 ± 0.1 (0.7)
ΔDiHS-triS	142.1 ± 4.4 (8.6)	0.1 ± 2.4 (0.7)	0.6 ± 1.0 (1.6)	0.7 ± 1.1 (1.8)	1.1 ± 1.1 (2.1)	1.9 ± 3.4 (3.0)	ND	0.7 ± 0.1 (0.6)
Total	1651.3 ± 112.3	139.4 ± 11.9	38.3 ± 19.2	35.5 ± 1.6	53.7 ± 18.1	64.0 ± 16.1	139.4 ± 16.6	124.1 ± 9.6

[1] These authors contributed equally to this work.
[2] To whom correspondence should be addressed (email kitagawa@kobepharma-u.ac.jp).

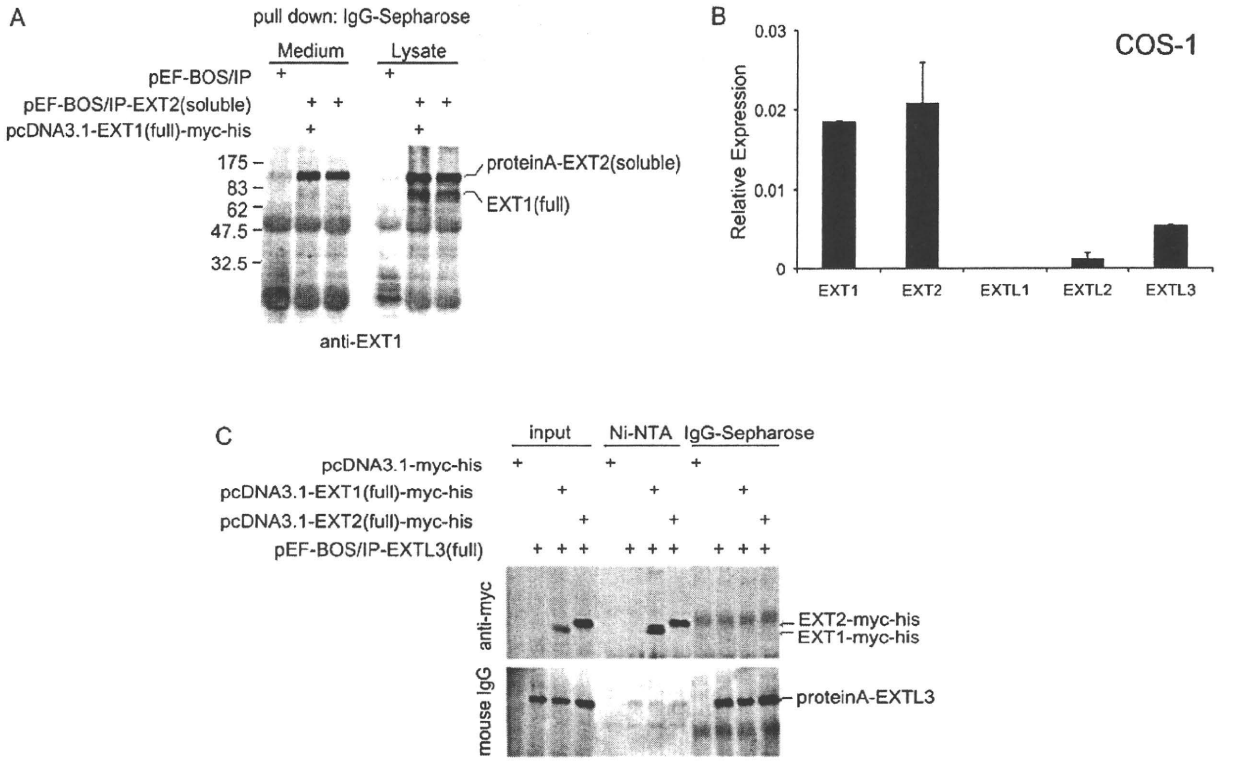

Figure S1 Purity of the secreted EXT2 proteins, expression levels of the *EXT* gene family in COS-1 cells and interactions between EXT2 and EXTL3

(**A**) pEF-BOS/IP-EXT2 or pcDNA3.1-EXT1(full)-myc-his expression plasmid (2 μg) was transfected into COS-1 cells on 60-mm-diameter dishes using Lipofectamine™ 2000 (Invitrogen). Two days after transfection, 2.5 ml of the medium was collected, and the secreted fusion protein was purified by incubation with 10 μl of IgG–Sepharose (GE healthcare) overnight at 4°C. The beads were recovered by centrifugation (1500 **g** for 2 min) were washed four times with PBS containing 0.1% Tween 20. In addition, COS-1 cells were solubilized with lysis buffer [20 mM Tris/HCl, pH 7.5, 1% (v/v) NP-40 (Nonidet P40), 0.15 M NaCl, 1 mM EDTA, 10% (v/v) glycerol and protease inhibitor cocktail] and cellular recombinant EXT2 proteins were purified by incubation with 10 μl of IgG–Sepharose overnight at 4°C. The beads were recovered by centrifugation (1500 **g** for 2 min) and washed four times with the lysis buffer. Each sample was resolved by SDS/PAGE (7.5% gels), transferred on to nitrocellulose membranes and incubated overnight with anti-EXT1 antibody (Abnova). The bound antibody was detected with anti-(mouse IgG) antibody conjugated to horseradish peroxidase. A representative blot is shown. Although expressed cellular EXT2 proteins interacted with endogenous EXT1, interactions between secreted recombinant EXT2 proteins and endogenous EXT1 proteins were not detected. Molecular masses are indicated on the left-hand side. (**B**) Expression levels of the *EXT* gene family in COS-1 cells were normalized to those of *GAPDH* (primers used are from the human *EXT* gene family; Supplementary Table S1). Results are means ± S.E.M. for two experiments. (**C**) pcDNA3.1-myc-his, pcDNA3.1-EXT1(full)-myc-his, pcDNA3.1(full)-EXT2-myc-his or pEF-BOS/IP-EXTL3(full) (2 μg) was transfected into HeLa cells on 60-mm-diameter dishes using Lipofectamine™ 2000 (Invitrogen). After 24 h, HeLa cells were solubilized with lysis buffer and cellular recombinant EXT2 proteins and Protein A–EXTL3 proteins were purified by incubation with 10 μl of Ni-NTA (Ni^{2+}-nitrilotriacetate)–agarose (Qiagen) and IgG–Sepharose respectively, for 1 h at 4°C. The beads were recovered by centrifugation (1500 **g** for 2 min) and washed four times with lysis buffer. Each sample was resolved by SDS/PAGE (7.5% gels), transferred on to nitrocellulose membranes and incubated overnight with anti-Myc antibody (Invitrogen) or anti-(mouse IgG) antibody. A representative blot is shown.

Received 15 January 2010/24 March 2010; accepted 9 April 2010
Published as BJ Immediate Publication 9 April 2010, doi:10.1042/BJ20100101

THE JOURNAL OF BIOLOGICAL CHEMISTRY VOL. 285, NO. 32, pp. 24717–24728, August 6, 2010

Two Golgi-resident 3′-Phosphoadenosine 5′-Phosphosulfate Transporters Play Distinct Roles in Heparan Sulfate Modifications and Embryonic and Larval Development in *Caenorhabditis elegans*[*] [S]

Received for publication, November 26, 2009, and in revised form, April 23, 2010 Published, JBC Papers in Press, June 6, 2010, DOI 10.1074/jbc.M109.088229

Katsufumi Dejima[‡§1], Daisuke Murata[‡§], Souhei Mizuguchi[‡§2], Kazuko H. Nomura[‡§], Tomomi Izumikawa[§¶], Hiroshi Kitagawa[§¶], Keiko Gengyo-Ando[§‖3], Sawako Yoshina[§‖], Tomomi Ichimiya[**], Shoko Nishihara[**], Shohei Mitani[§‖], and Kazuya Nomura[‡§4]

From the [‡]Department of Biology, Faculty of Sciences 33, Kyushu University, Fukuoka 812-8581, Japan, the [§]Core Research for Evolutional Science and Technology (CREST), Japan Science and Technology Agency (JST), 4-1-8 Hon-cho, Kawaguchi, Saitama 332-0012, Japan, the [¶]Department of Biochemistry, Kobe Pharmaceutical University, Higashinada-ku, Kobe 658-8558, Japan, the [‖]Department of Physiology, Tokyo Women's Medical University School of Medicine, Tokyo 162-8666, Japan, and the [**]Laboratory of Cell Biology, Department of Bioinformatics, Faculty of Engineering, Soka University, 1-236 Tangi-cho, Hachioji, Tokyo 192-8577, Japan

Synthesis of extracellular sulfated molecules requires active 3′-phosphoadenosine 5′-phosphosulfate (PAPS). For sulfation to occur, PAPS must pass through the Golgi membrane, which is facilitated by Golgi-resident PAPS transporters. *Caenorhabditis elegans* PAPS transporters are encoded by two genes, *pst-1* and *pst-2*. Using the yeast heterologous expression system, we characterized PST-1 and PST-2 as PAPS transporters. We created deletion mutants to study the importance of PAPS transporter activity. The *pst-1* deletion mutant exhibited defects in cuticle formation, post-embryonic seam cell development, vulval morphogenesis, cell migration, and embryogenesis. The *pst-2* mutant exhibited a wild-type phenotype. The defects observed in the *pst-1* mutant could be rescued by transgenic expression of *pst-1* and *hPAPST1* but not *pst-2* or *hPAPST2*. Moreover, the phenotype of a *pst-1;pst-2* double mutant were similar to those of the *pst-1* single mutant, except that larval cuticle formation was more severely defected. Disaccharide analysis revealed that heparan sulfate from these mutants was undersulfated. Gene expression reporter analysis revealed that these PAPS transporters exhibited different tissue distributions and subcellular localizations. These data suggest that *pst-1* and *pst-2* play different physiological roles in heparan sulfate modification and development.

Organogenesis, tissue morphogenesis, and cell growth require diverse types of extracellular sulfation. Sulfated molecules are crucial for the establishment of a hydrophilic extracellular environment and for intercellular signaling (1–8). In eukaryotes, Golgi-resident sulfotransferases transfer sulfates from an active sulfate, 3′-phosphoadenosine 5′-phosphosulfate (PAPS),[5] to membrane-associated and secreted molecules like glycosaminoglycans (GAGs) (9–11). The sulfation reaction yields 3′-phosphoadenosine 5′-phosphate (PAP) as a byproduct. Biochemical and cytological studies have revealed that PAPS is synthesized by PAPS synthase, a bifunctional enzyme found in the nucleus and/or cytosol but not in the Golgi apparatus (12–15). PAPS transporters transport PAPS from the cytosol into the Golgi lumen (16). Recent reports have demonstrated that PAPS/PAP concentrations in the Golgi apparatus are important for biosynthetic regulation of sulfated molecules, including heparan sulfate (HS) (17–20). Thus, understanding how PAPS metabolism is regulated by PAPS transporters *in vivo* will provide important insight into the mechanisms underlying developmental control of extracellular sulfation.

PAPS transporter activity was first demonstrated in rat liver Golgi-derived vesicles (16). The characterization of purified proteins involved in PAPS transport activity suggests that they act through an antiport mechanism (13, 21–24). Recently, two human PAPS transporter genes were cloned and named *PAPST1* (*Slc35b2*) (25) and *PAPST2* (*Slc35b3*) (26, 27). The *Drosophila slalom* gene, which encodes PAPST1, was identified as a segment polarity gene (28, 29). In zebrafish, mutations in *pinscher*, the gene encoding PAPST1, caused defects in skeletal development and axon sorting (30). Although the gene encoding PAPST2 showed genetic interactions with the genes that

* This work was supported by a grant-in-aid from the Japan Society for the Promotion of Science Fellows (to K. D.), a grant-in-aid for young scientists (B) (to S. M.), and Grant-in-Aid for Scientific Research B-21390025 (to H. K.) from the Ministry of Education, Culture, Sports, Science, and Technology (MEXT), Japan. This research was also supported by MEXT Grant-in-Aid for Scientific Research B-20370051 (to S. N.) and by the Core Research for Evolutional Science and Technology Program of the Japan Science and Technology Corp. (to K. N.).

[S] The on-line version of this article (available at http://www.jbc.org) contains supplemental Figs. S1–S4 and Table S1.

[1] Present address: Dept. of Genetics, Cell Biology and Development, University of Minnesota, Minneapolis, MN 55455.

[2] Present address: Dept. of Tumor Genetics and Biology, Graduate School of Medical Sciences, Kumamoto University, Kumamoto, Japan.

[3] Present address: Saitama University Brain Science Institute, Saitama 338–8570, Japan.

[4] To whom correspondence should be addressed: Dept. of Biology, Faculty of Sciences, Kyushu University, Fukuoka 812-8581, Japan. Tel. and Fax: 81-92-642-4613; E-mail: knomuscb@kyushu-u.org.

[5] The abbreviations used are: PAPS, 3′-phosphoadenosine 5′-phosphosulfate; DIC, differential interference contrast; DTC, distal tip cell; EGFP, enhanced green fluorescent protein; GFP, green fluorescent protein; GAG, glycosaminoglycan; HA, hemagglutinin; hPAPST, human PAPS transporter; HS, heparan sulfate; PAP, 3′-phosphoadenosine 5′-phosphate; Sqv, squashed vulva; NS, 2-*N*-sulfate; 2*S*, 2-*O*-sulfate; 6*S*, 6-*O*-sulfate.

encode HS modification enzymes in the fruit fly, its physiological roles are largely unknown (27).

The nematode *Caenorhabditis elegans* is a model organism that is well suited for developmental genetics because of its simple and well organized organs, including those of the reproductive, digestive, nervous, and epithelial tissue systems. The *C. elegans* genome contains orthologs of all the known enzymes involved in PAPS metabolism, including PAPS synthase (*pps-1*, T14G10.1), PAPS reductase (R53.1), Golgi-resident PAP phosphatase (Y6B3B.5), sulfate transporters (*sulp-2*, F14D12.5; *sulp-4*, K12G11.1) (31), and PAPS transporters (*pst-1*, M03F8.2; *pst-2*, F54E7.1). In addition, *C. elegans* expresses genes that are involved in the sulfation of tyrosine and HS but not chondroitin (32–36). This represents an advantage of using *C. elegans* over vertebrate species to investigate the role of PAPS metabolism in development. In vertebrates, chondroitin sulfate is required for chondrogenesis (2, 18, 19, 30), and defects in chondroitin sulfation obscure the importance of other sulfated molecules. Previous studies have demonstrated that extracellular sulfated molecules play pivotal roles in nervous system development, gonadal cell migration, cuticle formation, and embryogenesis in *C. elegans* (37–42). Most recently, *pst-1* alleles were shown to be required for viability and neuronal development (43).

In this study, we aimed to investigate the roles of PAPS transporters in development and morphogenesis. To that end, we isolated *C. elegans* deletion mutants of the PAPS transporters and analyzed the defects in development and morphogenesis.

EXPERIMENTAL PROCEDURES

Materials—[^{35}S]PAPS (1.59 Ci/mmol), GDP-[U-^{14}C]fucose (271 mCi/mmol), and CMP-[9-^{3}H]sialic acid (33.6 Ci/mmol) were purchased from PerkinElmer Life Sciences. UDP-[6-^{3}H]galactose (20 Ci/mmol), UDP-*N*-acetyl-D-[6-^{3}H]galactosamine (20 Ci/mmol), UDP-[1-^{3}H]glucose (20 Ci/mmol), GDP-[2-^{3}H]mannose (40 Ci/mmol), UDP-[U-^{14}C]glucuronic acid (300 mCi/mmol), and UDP-[U-^{14}C]xylose (264 mCi/mmol) were purchased from American Radiolabeled Chemicals Inc. (St. Louis, MO). UDP-*N*-acetyl-D-[U-^{14}C]glucosamine (293 mCi/mmol) was purchased from GE Healthcare.

C. elegans Strains—We used *C. elegans* N2 as the wild-type strain. Strains were maintained and cultured as described previously (44). We used strains carrying the following alleles and balancer chromosomes: *ayIs4* I (45), *tm3316* III, *syIs80* III (46), *jcIs1* IV (47), *tm3364* V, and *nT1[qIs51]* (IV;V). All except *pst-1(tm3364)* and *pst-2(tm3316)* were obtained from the Caenorhabditis Genetic Center, which is funded by the National Institutes of Health, National Center for Research Resources (NCRR).

Isolation of Worms with Deleted Alleles—Worms with deletions of the *pst-1(tm3364)* and *pst-2(tm3316)* alleles were isolated from pools of worms that had been mutagenized by using the trimethylpsoralen/UV method (48). The *pst-1(tm3364)* mutant contained an 1186-bp deletion and a 9-bp insertion, which removed the third and fourth exons of the gene and resulted in a frameshift mutation. These deleted exons are identical among the three *pst-1* splice variants. The *pst-1(tm3364)* deletion mutant expressed only one transmembrane region in the N terminus of the protein. The *pst-2(tm3316)* mutant contained a 296-bp deletion that removed part of the fifth exon, resulting in a frameshift mutation. This deletion mutant expressed only five transmembrane regions in the N terminus of the protein. The *pst-1* deletion mutant was balanced and maintained as the *pst-1(tm3364)/nT1[qIs51]* strain. A double *pst-1;pst-2* deletion mutant was maintained as the *pst-1(tm3364)/nT1[qIs51], pst-2(tm3316)* strain. To eliminate possible additional mutations, the *pst-1(tm3364)* and *pst-2(tm3316)* strains were back-crossed four and two times, respectively.

Analysis of GAGs—Freshly cultured nematodes were sonicated with a GE-70 ultrasonic processor (Branson Ultrasonics) and freeze-dried. The dried samples (136 mg of wild type, 72.8 mg of *pst-1*, and 182 mg of *pst-2*) were extracted with acetone and then treated with 6 ml of 1.0 M $NaBH_4$/0.05 M NaOH at 4 °C for 20 h. The reaction was stopped with the addition of acetic acid. The samples were adjusted to 5% trichloroacetic acid and centrifuged. The soluble fraction was extracted with ether. As shown previously (34, 49, 50), the amount of HS in *C. elegans* was extremely small; thus, for further processing, we added a carrier of 100 μg of shark cartilage chondroitin 6-*O*-sulfate (Seikagaku Corp.), which contained negligible amounts of non-sulfated disaccharides. The aqueous phase was adjusted to 80% ethanol. The resultant precipitate was dissolved in 50 mM pyridine acetate and subjected to gel filtration on a PD-10 column with 50 mM pyridine acetate as an eluent. The flow-through fraction was collected and evaporated. The dried samples were dissolved in water and applied to a column (7 ml) of cation-exchange resin AG 50W-X2 (H^+ form, Bio-Rad) pre-equilibrated with water. The unbound fraction, which contained the librated *O*-linked saccharides, was neutralized with 1 M NH_4HCO_3. The purified GAG fraction was digested with chondroitinase ABC or a mixture of heparitinases I and II, and then the digests were derivatized with 2-aminobenzamide and analyzed by high performance liquid chromatography as described previously (51).

Analysis of Embryonic Development—Four-dimensional microscopy was performed as described previously (49), except that embryos were mounted on a 2% agarose pad in M9 solution to examine the defects in the ventral cleft enclosure. This is because observation of the ventral cleft was difficult with embryos mounted on an 8-well printed microscopic glass slide (Matsunami Glass Inc.). To evaluate and compare the embryonic phenotypes of the mutants, embryos were dissected from the homozygous adult animals and cultured for 18 h in M9 at 20 °C.

Alkaline Bleach Assay—An alkaline bleach assay was performed basically as described (52). Ten adult hermaphrodites were transferred to a 5-μl M9 drop and placed on an 8-well glass slide followed by the addition of 2× alkaline hypochlorite solution (2 N NaOH, 80% NaOCl solution (10% available chlorine)). For the "time to stop thrashing," we recorded the time starting from the addition of hypochlorite and ending when all worms stopped thrashing.

Plasmid Construction—We generated plasmids that attached enhanced green fluorescent protein (*egfp*) or *mCherry* gene to the ends of different PAPS transporter or reporter genes. Plasmids were constructed on a pFX_EGFPT vector

backbone, essentially as described previously (53, 54), and named according to the gene they carried: $P_{pst\text{-}1a}$::*egfp*, $P_{pst\text{-}1b,c}$::*egfp*, *pst-1ab(fl)*::*egfp*, *pst-1c(fl)*::*egfp*, $P_{pst\text{-}2}$::*egfp*, *pst-2a(fl)*::*egfp*, *pst-2b(fl)*::*egfp*, $P_{unc\text{-}119}$::*egfp*, and $P_{rgef\text{-}1}$::*egfp* ($P_{pst\text{-}1a}$ stands for *pst-1a* promoter and *fl* stands for full length (supplemental Figs. 1 and 2)). Briefly, cDNAs were amplified by reverse transcription-PCR from total RNA of wild-type *C. elegans* with specific primers tagged with the NotI restriction site. We inserted the cDNA fragments digested with NotI into the $P_{dpy\text{-}7}$::*egfp* or the $P_{dpy\text{-}7}$::*mCherry* plasmid to create $P_{dpy\text{-}7}$::*pst-1b*::*egfp*, $P_{dpy\text{-}7}$::*pst-2a*::*egfp*, and $P_{dpy\text{-}7}$::*aman-2*::*mCherry* (15, 55). Similarly, cDNAs were amplified by reverse transcription-PCR from total RNA of human prostate cancer (LNCaP) cells with specific primers tagged with NotI restriction sites, and cDNA fragments digested with NotI were cloned into the $P_{eft\text{-}4}$::*Venus* plasmid to make $P_{eft\text{-}4}$::*hPAPST1*::*Venus* and $P_{eft\text{-}4}$::*hPAPST2*::*Venus* (53). To make the tissue-specific *pst-1b*::*egfp* and *pst-2a*::*egfp* expression constructs, $P_{dpy\text{-}7}$::*pst-1a*::*egfp* and $P_{dpy\text{-}7}$::*pst-2a*::*egfp* were digested with NotI to yield the *pst-1a* and *pst-2a* sequences, respectively. These were cloned into $P_{myo\text{-}3}$::*egfp*, $P_{unc\text{-}119}$::*egfp*, and $P_{rgef\text{-}1}$::*egfp* plasmids. The plasmids for the yeast expression system were prepared using the GATEWAY™ cloning system (Invitrogen) as described previously (25–27). We used two steps of attB adaptor PCR for preparation of the attB-flanked PCR products. The first PCR step was performed with gene-specific primers, and the second PCR step was performed with attB adaptive primers. The PCR products of *pst-1a* and *pst-2* were cloned into pDONR™201. Then each construct was converted into a yeast expression vector, YEp352GAP-II, which was inserted into additional attB cassettes sequences and three influenza HA epitope tag sequences at the position of the multicloning site of YEp352GAP-II. YEp352GAP-II-*pst1a-HA* and YEp352GAP-II-*pst2-HA* plasmids were transformed into yeast. DNA sequence analysis was performed with the Prism 3130 Genetic Analyzer (Applied Biosystems). The PCR primers used in this section are listed in Table S1.

DNA Microinjection—Microinjections were performed as described by Mello and Fire (56). Expression constructs under the control of the *eft-4* promoter or other promoters were injected at 2–10 or 30 ng/μl, respectively, with co-injection of a tissue-specific marker, $P_{tph\text{-}1}$::*dsred* or $P_{aman\text{-}2}$::*aman-2*::*mCherry* at 20 ng/μl and/or *rol-6(gf)* at 80 ng/μl.

Subcellular Fractionation of Yeast and Transport Assay—Golgi-rich subcellular fractionation and nucleotide sugar transport assays were performed as described previously (25–27). Each YEp352GAP-II-*pst-1a-HA* and YEp352GAP-II-*pst-2-HA* plasmid was transformed into yeast (*Saccharomyces cerevisiae*) strain W303-1a (*MATa, ade2–1, ura3–1, his3–11,15, trp1–1, leu2–3,112,* and *can1–100*) by the lithium acetate procedure. These transformed yeast cells were grown at 30 °C in a synthetic defined medium lacking uracil. Yeast cells were converted into spheroplasts, homogenized, and fractionated to yield a 100,000 × *g* Golgi-rich subcellular fraction. Then, each Golgi-rich membrane fraction (200 or 100 μg of protein) was incubated in 50 μl of reaction buffer (20 mM Tris-HCl, pH 7.5, 0.25 M sucrose, 5.0 mM $MgCl_2$, 1.0 mM $MnCl_2$, and 10 mM 2-mercaptoethanol) that contained various substrates (mixture of radiolabeled and cold substrate) at 25 °C for 5 min. After incubation, the radioactivity incorporated in the Golgi-rich subcellular fractionation was trapped using a 0.45-μm nitrocellulose filter (Advantec MFS) and measured using liquid scintillation. The amount of radioactivity incorporated was calculated as the difference from the background value obtained from the same assay at 0 min for each sample.

Western Blot Analysis—The Golgi-rich subcellular fraction samples were suspended in 3× SDS sample buffer (New England Biolabs) and incubated 4 °C for 16 h. The samples were subjected to 10% SDS-polyacrylamide gel electrophoresis. The membrane to which the separated proteins were transferred was probed with anti-HA monoclonal antibody (Santa Cruz Biotechnology, Santa Cruz, CA) and horseradish peroxidase-conjugated anti-mouse IgG antibody and stained with ECL Plus (GE Healthcare).

Analysis of Subcellular Localization of PST-1·EGFP and PST-2·EGFP—To determine subcellular localization of the PST-1·EGFP protein, transgenic animals carrying extrachromosomal arrays of $P_{dpy\text{-}7}$::*pst-1b*::*egfp* and $P_{dpy\text{-}7}$::*aman-2*::*mCherry* were freeze-cracked and fixed in methanol for 5 min at −20 °C (57). After blocking with TBST (Tris-buffered saline containing 0.2% Tween 20), samples were incubated with the anti-GFP monoclonal antibody (1:100 dilution, mFX73; Wako Pure Chemical Industries) and anti-DsRed polyclonal antibody (1:100 dilution, Clontech) at room temperature for 2 h. Then, samples were washed twice with TBST and incubated at room temperature for 2 h with Alexa 488- or 594-conjugated anti-mouse IgG (H+L) (Molecular Probes) and/or Alexa 594-conjugated anti-rabbit IgG secondary antibody (Molecular Probes), diluted 1:200. Subcellular localization of the PST-2·EGFP protein was determined by examining transgenic animals that carried extrachromosomal arrays of *pst-2a(fl)*::*egfp* and $P_{aman\text{-}2}$::*aman-2*::*mCherry*. The specimens were observed on a Zeiss LSM510 system (Carl Zeiss). The extent of co-localization of PST-1·EGFP and PST-2·EGFP with AMAN-2·mCherry was determined as the percent intensity of the co-localized signal relative to the total GFP-specific signal using the colocalization threshold plug-in within NCBI Image J software.

RESULTS

Identification of C. elegans PAPS Transporter Genes pst-1 and pst-2—Only a single orthologous gene for each human PAPS transporter is found in the *C. elegans* genome: *pst-1* (M03F8.2) and *pst-2* (F54E7.1) (54, 33). The amino acid sequence of the human PAPS transporter-1 (hPAPST1) is 40.0, 40.5, and 36.3% identical to that of PST-1a, PST-1b, and PST-1c, respectively (supplemental Fig. S1*A*). On the other hand, the human PAPS transporter-2 (hPAPST2) amino acid sequence is 40.3 and 30.1% identical to that of PST-2a and PST-2b, respectively (supplemental Fig. S2*A*). The Web tool Phobius (58, 59) predicted that all the PST-1 variants possess nine transmembrane regions, whereas PST-2a and PST2b possess 10 and six transmembrane regions, respectively (supplemental Figs. S1*A* and S2*A*). The *C. elegans* genome database (Wormbase) indicates that the *pst-1* and *pst-2* loci encode three and two splice variants, respectively, and both loci are included in operons (OP5092 and OP3316) (supplemental Figs. S1*B* and S2*B*).

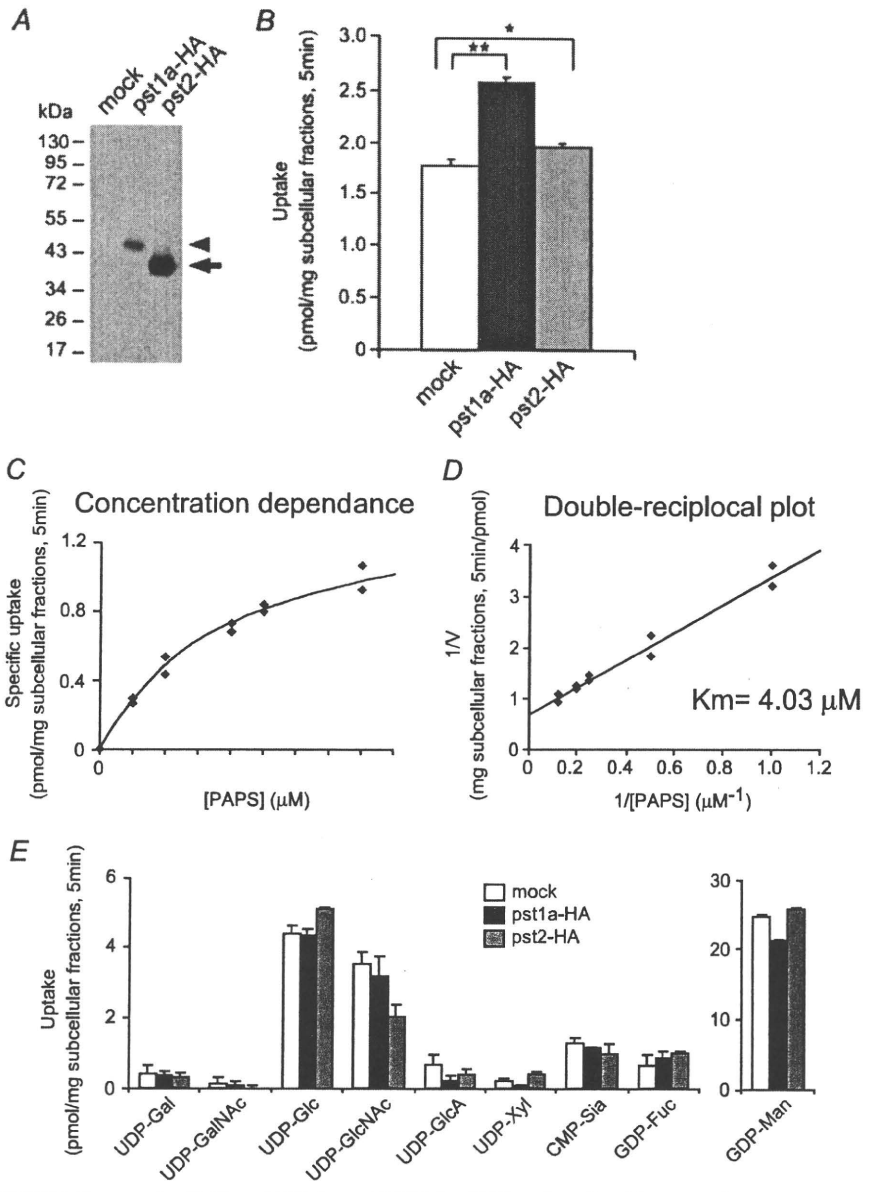

FIGURE 1. **Transport activities of PST-1a and PST-2 for PAPS and nucleotide sugars by yeast expression.** *A*, Western blot analysis of the Golgi-rich subcellular fraction prepared from yeast cells expressing mock (*left lane*), HA-tagged PST-1a (*center lane*), and HA-tagged PST-2 (*right lane*) using anti-HA monoclonal antibody. The loaded amount of subcellular fraction proteins was 5 μg from the cells expressing mock or HA-tagged PST-1a and 0.5 μg from the cells expressing HA-tagged PST-2. The *arrowhead* and *arrow* indicate HA-tagged PST-1a and HA-tagged PST-2, respectively. *B*, PAPS uptake of PST-1a and PST-2. 200 μg of Golgi-rich subcellular fraction for each sample was incubated in 50 μl of reaction buffer containing 5 μM PAPS (mixture of 2 μM [^{35}S]PAPS and 3 μM PAPS) at 25 °C for 5 min, and the incorporated radioactivity was measured. Values shown are the mean ± S.D. obtained from two independent experiments. *Open bar*, mock; *solid bar*, PST-1a-HA; *gray bar*, PST-2-HA. *, $p < 0.05$; **, $p < 0.001$; assessed by two-tailed Student's *t* test. *C*, substrate concentration dependence of PST-1a. 200 μg of Golgi-rich subcellular fraction for each sample was incubated in 50 μl of reaction buffer containing different concentrations of [^{35}S]PAPS at 25 °C for 5 min, and the incorporated radioactivity was measured. Specific uptake of PST-1a was calculated by subtracting the value of the mock uptake from the values of PST-1a-HA uptake. *D*, double-reciprocal plot used to determine the K_m value of PST-1a. *E*, nucleotide sugar uptake of PST-1a and PST-2. 100 μg of Golgi-rich subcellular fraction for each sample was incubated in 50 μl of reaction buffer containing 2 μM various nucleotide sugars at 25 °C for 5 min, and the incorporated radioactivity was measured. Values shown are the mean ± S.D. obtained from two independent experiments. *Open bar*, mock; *solid bar*, PST-1a-HA; *gray bar*, PST-2-HA.

Substrate Specificities of PST-1 and PST-2 Proteins Expressed in Yeast Cells—To determine the functional properties of PST-1 and PST-2, a heterologous yeast expression system was used (25–27). Western blot analysis demonstrated that PST-1a and PST-2 proteins were both expressed in the yeast P100 membrane fraction (Fig. 1*A*). The P100 fraction derived from yeast cells expressing PST-1a exhibited significant PAPS transport activity (Fig. 1*B*). The substrate concentration dependence on PAPS transport by PST-1a is shown in Fig. 1, *C* and *D*. The apparent K_m value of PST-1a was estimated to be 4.03 μM. PST-2 protein also exhibited statistically significant transport activity (Fig. 1*B*). However, the K_m value was not determined, because of its small transport activity. No significant difference was observed in transport activity of PST-1a and PST-2 for nucleotide sugars (Fig. 1*E*). These results suggest that the PST-1 and PST-2 proteins are PAPS-specific transporters.

Isolation of pst-1 and pst-2 Deletion Mutants—To gain insight into the physiological roles of PAPS transporters in *C. elegans*, we isolated strains with deletions in each of the *pst* genes from a library of trimethylpsoralen/UV-mutagenized worms by PCR screening. We isolated mutants that were predicted to have large transmembrane deletions in both alleles and thus likely to lack nucleotide sugar or PAPS transport activity (supplemental Figs. S1*A* and S2*A*). The isolated *pst-1(tm3364)* homozygotes had pleiotropic defects and an embryonic lethal phenotype (Fig. 2*B* and Table 1; also see below). In contrast, the isolated *pst-2(tm3316)* homozygotes were viable and fertile (Fig. 2*C* and Table 1; also see below) but had slightly reduced brood sizes (not shown).

Reduced HS Sulfation in pst-1(tm3364) and pst-2(tm3316) Mutant Worms—Next, we examined HS sulfation in the PAPS transporter mutants. Because of the embryonic lethality of the *pst-1*

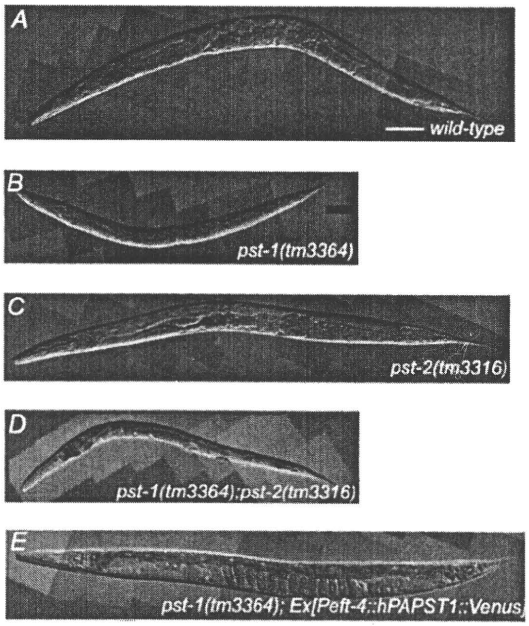

FIGURE 2. ***pst-1(tm3364), pst-2(tm3316),* and *pst-1(tm3364);pst-2(tm3316) C. elegans* mutants and transgenic rescue by hPAPST1.** *A–D*, representative DIC images of adult *C. elegans* wild type (*A*), *pst-1(tm3364)* mutant (*B*), *pst-2(tm3316)* mutant (*C*), and *pst-1(tm3364);pst-2(tm3316)* double mutant (*D*). The *pst-1(tm3364);pst-2(tm3316)* double mutant showed morphological features similar to those of the *pst-1(tm3364)* mutant. *E*, representative DIC image of an adult *pst-1(tm3364)* mutant expressing the *hPAPST1* transgene under the *eft-4* promoter ($P_{eft\text{-}4}$::*hPAPST1::Venus* construct). *Scale bar* = 100 μm.

TABLE 1

Summary of the phenotypes of PAPS transporter mutant animals

+, Abnormality was observed; + +, severe abnormality was observed; −, abnormality was not observed; ND, not determined.

Phenotype	*pst-1(tm3364)*	*pst-2(tm3316)*	*pst-1, pst-2*
Embryonic			
AB/P1 asymmetric cell division	−	−	ND
Cytokinesis	−	−	ND
EMS cell division	+	−	ND
Ea and Ep cell ingression	−	−	ND
Ventral enclosure	+	−	ND
Epidermal elongation	+	−	+
Larval			
Cuticle formation	+	−	+ +
Vulval morphology	+	−	+
Seam cell morphology	+	−	+
DTC migration	+	−	+

mutant, liquid culture samples containing *pst-1(tm3364)/nT1[qIs51]* heterozygous and *pst-1(tm3364)/pst-1(tm3364)* homozygous animals were used for biochemical analysis. For the *pst-2* mutant, liquid culture samples containing the *pst-2(tm3316)* homozygous animals were used. In wild-type worms, HS disaccharide analysis revealed the expected profile (Table 2) (15, 34, 35, 41). In both *pst-1* and *pst-2* mutant worms, the number of nonsulfated units increased, and the number of sulfated units decreased; this suggested that both *pst-1* and *pst-2* were involved in sulfation of HS *in vivo*. Notably, the disaccharide profile of the *pst-1* mutants was different from that of the *pst-2* mutant. The levels of trisulfated disaccharide units (ΔHexA(2*S*)α1−4GlcN(NS,6*S*)) were reduced in the *pst-1*

TABLE 2

Disaccharide composition of HS from *C. elegans* wild-type (N2) and mutant (*pst-1* and *pst-2*) strains

Disaccharide[a]	N2	*pst-1*[b]	*pst-2*[c]
	pmol/mg HS (%)		
ΔHexAα1−4GlcNAc[c]	23.6 ± 0.3 (47)	35.3 ± 0.8 (69)	22.6 ± 2.7 (71)
ΔHexAα1−4GlcNAc(6*S*)	4.8 ± 1.2 (10)	5.3 ± 3.0 (10)	1.5 ± 0.3 (5)
ΔHexAα1−4Glc(NS)	12.9 ± 1.7 (26)	8.2 ± 3.2 (17)	4.9 ± 2.3 (15)
ΔHexA(2*S*)α1−4Glc(NS)	7.2 ± 1.9 (14)	1.6 ± 0.5 (3)	1.7 ± 1.0 (5)
ΔHexA(2*S*)α1−4Glc(NS,6*S*)	1.6 ± 0.5 (3)	0.7 ± 0.1 (1)	1.0 ± 0.4 (3)
Total disaccharide	50.1 ± 3.5	51.1 ± 5.9	31.7 ± 3.6
Sulfation degree[d]	0.74	0.37	0.40

[a] ΔHexAα, Glc, and GlcNAc represent unsaturated hexuronic acid, glucosamine, and *N*-acetylglucosamine, respectively.
[b] Liquid culture samples containing *pst-1(tm3364)/nT1[qIs51]* heterozygotes and *pst-1(tm3364)/pst-1(tm3364)* homozygotes were used.
[c] Liquid culture samples containing only *pst-2(tm3316)* homozygous animals were used.
[d] Sulfation degree is expressed as the average number of sulfate groups/disaccharide unit.

mutant worms, but they were not affected in the *pst-2* mutant worms compared with the controls (N2 worms). Conversely, the levels of ΔHexAα1−4GlcNAc(6*S*) were not affected in the *pst-1* mutant worms, but they were reduced in the *pst-2* mutant worms compared with controls. These results suggest that sulfation patterns of HS depend on both PST-1 and PST-2 activity.

Defects in pst-1 Are Rescued by Expression of Human PAPS Transporter-1 but Not Human PAPS Transporter-2—We performed rescue experiments in *pst-1* mutant worms by injecting plasmid constructs that carried wild-type genes under the *eft-4* promoter, which is active in almost all cells (41). Transgenic expression of *pst-1b::egfp* in *pst-1(tm3364)* animals rescued all the observed defects. This suggested that the *eft-4* promoter was sufficient to drive expression of constructs in cells that lacked PST-1 function (not shown). hPAPST1 and hPAPST2 are well characterized human Golgi-resident PAPS transporters (25, 26, 27). Transgenic expression of *hPAPST1::Venus* also rescued all of the defects observed in *pst-1(tm3364)* animals; this suggested that PST-1 is the homolog of the human PAPS transporter-1 (Fig. 2*E*). However, expression of *hPAPST2::Venus* did not rescue any of the defects, although we confirmed that the hPAPST2 protein was expressed in the transgenic worms (data not shown).

PST-1 Is Required for Cuticle Formation—Homozygous *pst-1(tm3364)* embryos from the *pst-1(tm3364)* heterozygous hermaphrodites hatched and developed into small, fragile L3 (5%), L4 (44%), or adult (51%) animals with impaired cuticles (n = 82; Fig. 2*B*). In contrast, development of *pst-2(tm3316)* homozygotes was similar to that of the wild type (Fig. 2*C*). Although *pst-1(tm3364)* mutant larvae exhibited apparently normal locomotion nematode growth medium agar plate during the L3 stage, they exhibited "skiddy" locomotion during the L4 to adult stages (not shown). A previous report showed that skiddy locomotion is correlated with a defect in cuticle formation (52). Differential interference contrast (DIC) microscopy analysis showed that the cuticle started to become irregular in the early L3 stage (compare Fig. 3, *A* and *C*). During the L4 to adult stages, the cuticle became more severely abnormal, resulting in defective molting with some blisters (compare Fig. 3, *B* and *D*). The old, unshed cuticle remained attached to the body in various places. In contrast, no cuticle abnormality was observed in the *pst-2(tm3316)* mutant worms. We also examined cuticle

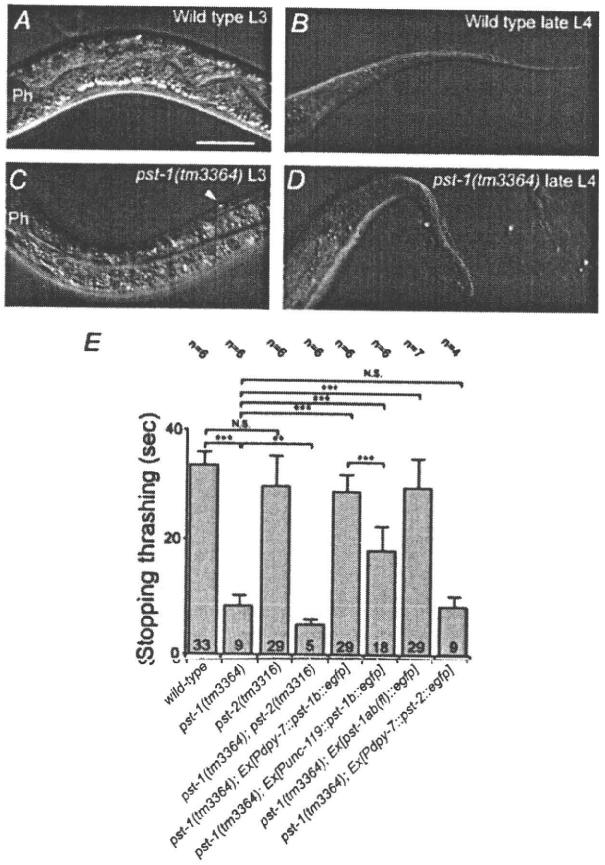

FIGURE 3. **Cuticle defect phenotype in *pst-1(tm3364)*, *pst-2(tm3316)*, and *pst-1(tm3364);pst-2(tm3316)* *C. elegans* mutant adult animals.** *A–D*, representative DIC images of regions behind the head (*A* and *C*) and tail (*B* and *D*) of wild-type L3 (*A*), wild-type late-L4 (*B*), *pst-1(tm3364)* mutant L3 (*C*), and *pst-1(tm3364)* mutant late-L4 larvae (*D*). *Ph*, posterior pharyngeal bulb; *arrowhead* (in *C*), in *pst-1(tm3364)* L3 larvae, some small protuberances of outer cuticle were observed, which were not observed in wild-type animals. During mid-L4 to the young adult stage, *pst-1(tm3364)* mutant animals showed abnormal molting (*D*). *Bar* = 30 μm. *E*, analysis of alkaline bleach sensitivity. The time to stop thrashing in alkaline bleach solution was an indicator of cuticle fragility. The *pst-1(tm3364)* mutant animals were more fragile (stopped faster) than the wild-type animals. In contrast, *pst-2(tm3316)* mutants showed cuticle fragility similar to wild-type animals. The *pst-1(tm3364);pst-2(tm3316)* double mutant animals were more fragile than the *pst-1(tm3364)* single mutant animals. In transgenic *pst-1(tm3364)* mutant animals that carried an extrachromosomal array of $P_{dpy\text{-}7}$::*pst-1b*::*egfp* or $P_{unc\text{-}119}$::*pst-1b*::*egfp*, the cuticle fragility was restored to the wild-type level, but the former was slightly more fragile than the latter. In transgenic *pst-1(tm3364)* mutant animals that carried an extrachromosomal array of $P_{dpy\text{-}7}$::*pst-2*::*egfp*, the cuticle fragility was similar to that of *pst-1(tm3364)* mutants without the transgene. *Ex*, extrachromosomal array; *N.S.* = not significant. **, $p < 0.01$; ***, $p < 0.001$; assessed by two-tailed Student's *t* test.

fragility by testing alkaline bleach sensitivity (52). Consistently, mutant *pst-1(tm3364)* worms exhibited very fragile cuticles (rapidly stopped moving in the alkaline solution), whereas mutant *pst-2(tm3316)* worm cuticle fragility was similar to that of the wild-type animals (Fig. 3*E*).

PST-1 Is Required for Vulval Morphogenesis—DIC analysis showed that almost all *pst-1* knock-out animals exhibited various forms of disorganized vulval morphology. In 79% (n = 39) of *pst-1(tm3364)* mutant mid-L4 larvae, the vulva contained some abnormally positioned cells, which resulted in a longer invagination along the anterior-posterior axis or a small, ectopic invagination (Fig. 4, *A* and *B*). In 16% (n = 8) of *pst-1(tm3364)* mid-L4 larvae, vulval cells were arranged relatively normally but exhibited a collapsed invaginated space (Fig. 4*A*, *middle*) similar to that observed in the squashed vulva (Sqv) phenotype caused by a deficiency in chondroitin glycosaminoglycan synthesis (44, 49, 60, 61). The vulval architecture in the *pst-1(tm3364)* mutant was visualized with the transgenic expression of *ajm-1*::*gfp*, an adherence junction marker of epithelial and vulval cells. This showed a disturbance during the mid-L4 stage (Pn.pxxx stage) (Fig. 4*C*). A large fraction (43%) of the *pst-1(tm3364)* mutant animals exhibited a fragmented vulva, and 17.4% (n = 23) exhibited incorrectly positioned cells. This observation suggested that vulval cell migration and orientation are affected in *pst-1(tm3364)* mutants. A LIM class homeobox gene, *lin-11*, which is involved in specific cell fates of vulva cell types, was transgenically expressed with the $P_{lin\text{-}11}$::*gfp* construct. In wild-type secondary cells, *lin-11* typically shows an asymmetric expression pattern (46) (Fig. 4*D*). In *pst-1(tm3364)* mutants, the asymmetric *lin-11*::*gfp*(*syIs80*) expression pattern was irregular (Fig. 4*E*, 33.3%, n = 15) at the L3 stage (Pn.pxx stage), and expression levels were drastically reduced at the mid-L4 stage (Pn.pxxx stage) (Fig. 4*F*, 100%, n = 20). However, in VC motor neurons, *lin-11*::*gfp* expression was undisturbed (Fig. 4*D*).

Additionally, the expression levels of GFP were not affected in worms expressing $P_{egl\text{-}17}$::*gfp* where *egl-17* encodes a fibroblast growth factor family member, which is specifically expressed in secondary cells at the Pn.pxxx stage. However, the patterning of cells that expressed $P_{egl\text{-}17}$::*gfp* was affected at this stage (data not shown). These results suggested that secondary cell fate is adopted in *pst-1(tm3364)* and that PST-1 is involved in vulval morphogenetic events via regulation of *lin-11* expression.

PST-1 Is Required for Post-embryonic Seam Cell Development and Distal Tip Cell (DTC) Migration—Disruption of the *pst-1* gene resulted in abnormal seam cell development (see supplemental Fig. S3 and the legend for details). The results suggested that *pst-1* is involved in post-embryonic seam cell development. In addition to epithelial defects, *pst-1* mutant animals were also defective in DTC migration. During the L4 stage in most wild-type animals, two DTCs that reached the dorsal side migrated along the dorsal body wall muscles toward the middle of the animal (supplemental Fig. S3*E*). In *pst-1(tm3364)* mutant larvae, 26.4% (n = 49) of anterior and 45.6% (n = 48) of posterior DTCs failed to migrate along the dorsal side and remained on the ventral side in the early to mid-L4 stage (supplemental Fig. S3, *F* and *G*). In *pst-2(tm3316)* mutant larvae, no abnormalities in seam cell development or DTC migration were observed (supplemental Fig. S3*G*).

PST-1 Is Required during Embryogenesis for Oriented EMS Cell Division, Neuroblast Migration, and Epidermal Elongation—The second generation (F1) of *pst-1(tm3364)* homozygous embryos, which is predicted to lack both maternal and zygotic *pst-1* activity, displayed a fully penetrant embryonic lethal phenotype (Fig. 5*A*). This suggested that the first generation of *pst-1(tm3364)* homozygous embryos grew to adults because maternally supplied molecules rescued the deficient embryos. Two-thirds (67%) of the *pst-1(tm3364)* F1 embryos displayed

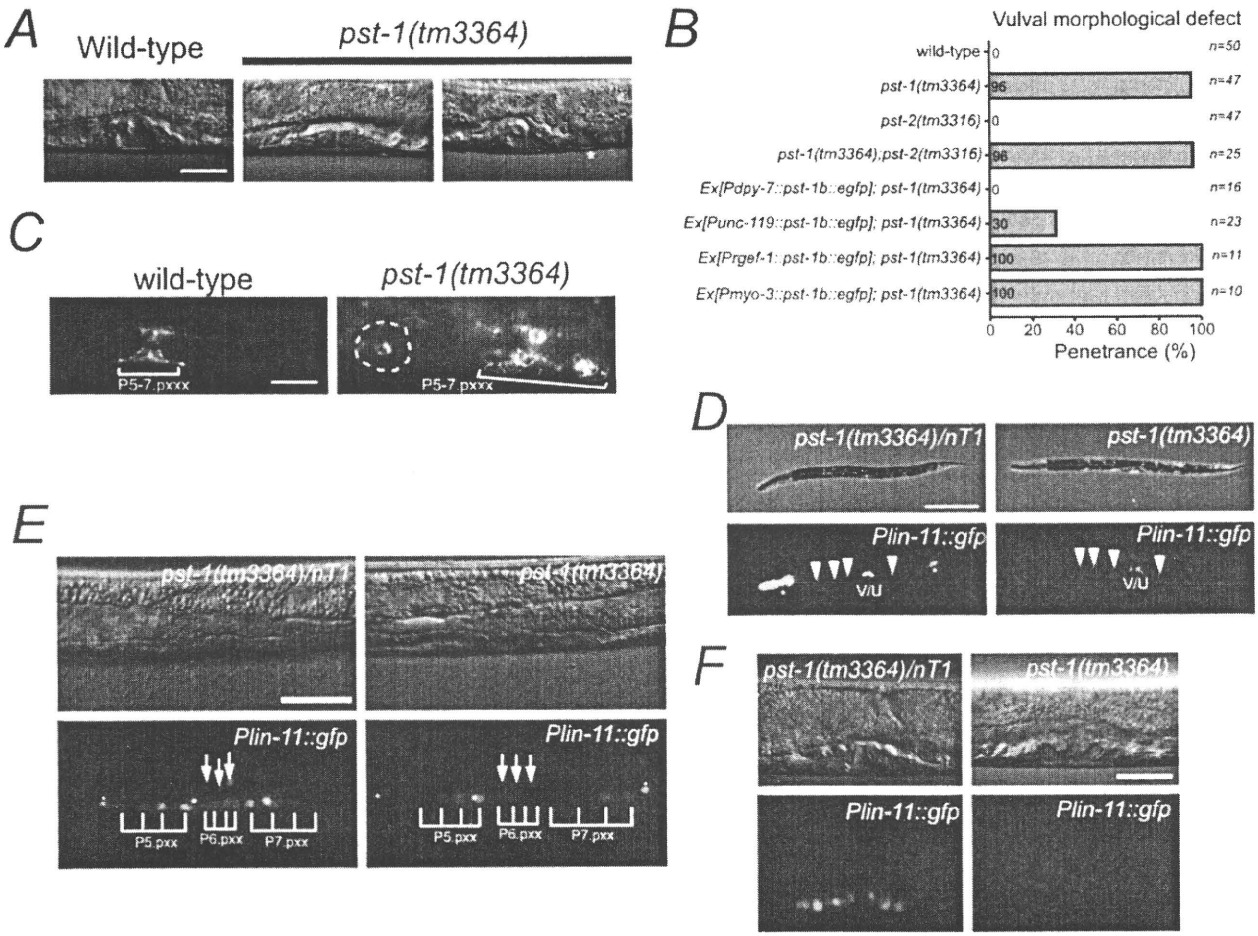

FIGURE 4. **Vulval defects of the *pst-1(tm3364)* mutant.** *A*, wild-type vulva forms an invagination space that looks like a pointed hat during early to mid-L4 stage (*left*). The *pst-1(tm3364)* mutation induced a collapse of the vulval invagination space (*middle*). In the mid-L4 stage, the *pst-1(tm3364)* vulva exhibited an ectopic invagination space (*asterisk, right panel*). *Scale bar* = 20 μm. *B*, penetrance in several genetic backgrounds of vulval morphological defects, including the squashed vulva and inappropriate vulval cell positioning. *Ex*, extrachomosomal array. *C*, the vulval structures of wild-type (*left*) and *pst-1(tm3364)* homozygote (*right*) animals were visualized with AJM-1-GFP. Incorrectly positioned cells are circled with a *yellow dashed line*. *Scale bar* = 20 μm. *D*, DIC and fluorescence images of *pst-1(tm3364)/nT1* (*left*) and *pst-1(tm3364)* homozygote (*right*) mid-L4 animals that expressed P_{lin-11}::*gfp*. The *pst-1(tm3364)/nT1* animals with the *syIs80* transgene showed P_{lin-11}::*gfp* expression patterns similar to those of wild-type animals (data not shown). The GFP signals derived from the *nT1[qIs51]* balancer chromosome are indicated with *asterisks*. *Arrowheads* indicate VC motor neurons, and *V/U* indicates P_{lin-11}::*gfp* expression in the vulva and uterus. *Bar* = 200 μm. *E*, DIC and fluorescence images of *pst-1(tm3364)/nT1* (*left*) and *pst-1(tm3364)* homozygote (*right*) vulvas during the L3 stage (Pn.pxx stage). GFP signals from VC motor neurons are indicated with *asterisks*. GFP signals from the uterus are indicated with *arrows*. *Bar* = 25 μm. *F*, DIC and fluorescence images of *pst-1(tm3364)/nT1* (*left*) and *pst-1(tm3364)* (*right*) homozygote vulvas during the mid-L4 stage (Pn.pxxx stage). *Bar* = 25 μm.

severe morphogenetic defects that resulted in disorganized morphology before the early stage of elongation; the other one-third (33%) displayed relatively mild morphogenetic defects that resulted in developmental arrest during the elongation stage. This embryonic phenotype was reminiscent of the disruption of HS synthesis by *rib-1* and *rib-2* knock-outs (40, 41, 62) or the disruption of PAPS synthesis (15). This supports the notion that *pst-1* is involved in HS sulfation during embryonic development. In contrast, embryos that lacked *pst-2* activity displayed little or no overt embryonic lethality (Fig. 5*A*). Analysis of *pst-1(tm3364)* F1 embryos by DIC optics revealed that none (n = 23) were affected in the initial step of gastrulation (ingression of Ea and Ep cells), but a small fraction of them were affected in EMS cell division orientation (6.9%, n = 29; Fig. 5, *B* and *C*). In wild-type embryonic morphogenesis, ventral neuroblasts migrated toward the ventral cleft created by the ingression of mesodermal cells, where they formed a substrate for the epidermis during ventral enclosure (63). In *pst-1(tm3364)* F1 embryos that exhibited severe morphogenetic defects, ventral enclosure failed, resulting in an unenclosed ventral surface (Fig. 5, *D* and *F*), suggesting that PST-1 was involved in neuroblast migration in the early morphogenesis phase. The *pst-1(tm3364)* F1 embryos that underwent normal ventral enclosure elongated to variable lengths ranging from 1.5- to 3-fold increases in size and then retracted, resulting in a swollen body morphology (Fig. 5, *E* and *G*).

Differential Expression Patterns of pst-1 and pst-2—To determine the localization of *pst-1* and *pst-2*, we injected four types of *pst-1* and three types of *pst-2* transgene expression vectors into wild-type animals. (Constructs and expression patterns summarized in supplemental Figs. S1*C* and S2*C* and Table 3.) In animals that carried the *pst-1ab(fl)*::*egfp*, *pst-1c(fl)*::*egfp*, and

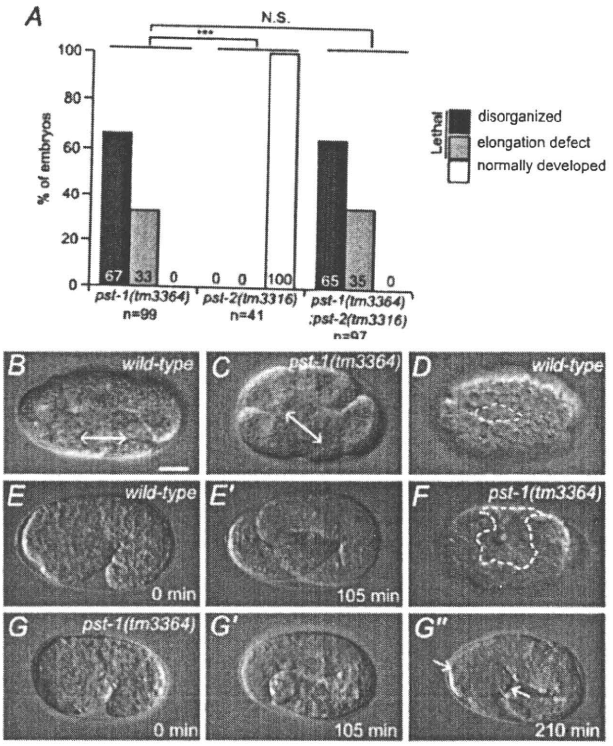

FIGURE 5. **Embryonic phenotypes of *pst-1* and *pst-2*.** *A*, percentage of embryonic mutant phenotypes in *pst-1(tm3364)*, *pst-2(tm3316)*, and double *pst-1(tm3364);pst-2(tm3316)* mutants. *N.S.*, not significant. ***, $p < 0.001$. *B* and *C*, EMS cell division axis is affected in *pst-1(tm3364)* embryos. In wild-type embryos at the 6-cell stage, EMS cells divide along the anterior/posterior axis (*bidirectional arrow* (*B*)). In *pst-1(tm3364)* mutant embryos at the 6-cell stage, the axis of EMS division is skewed (*bidirectional arrow* (*C*)). *D* and *F*, DIC images of wild-type (*D*) and *pst-1(tm3364)* (*F*) embryos at the ventral cleft enclosure stage. The *dashed lines* indicate the edges of an unenclosed ventral surface. *E–G"*, time lapse analysis of wild-type (*E* and *E'*) and *pst-1(tm3364)* (*G* and *G"*) embryos during the elongation stage. *Arrows* indicate swollen body morphology. *Scale bar* = 10 μm.

TABLE 3
Summary of the expression patterns of PAPS transporter genes

Reporter construct	Expression pattern
$P_{pst\text{-}1a}$::*egfp*	Ubiquitous
$P_{pst\text{-}1bc}$::*egfp*	Epidermis (amphid sheath cells, hypodermis, seam cells)
pst-1-ab(fl)::*egfp*	Epidermis (amphid sheath cells, hypodermis, seam cells)
pst-1c(fl)::*egfp*	Epidermis (amphid sheath cells, hypodermis, seam cells)
$P_{pst\text{-}2}$::*egfp*	Intestine, gland cells
pst-2a(fl)::*egfp*	Intestine, gland cells
pst-2b(fl)::*egfp*	No expression

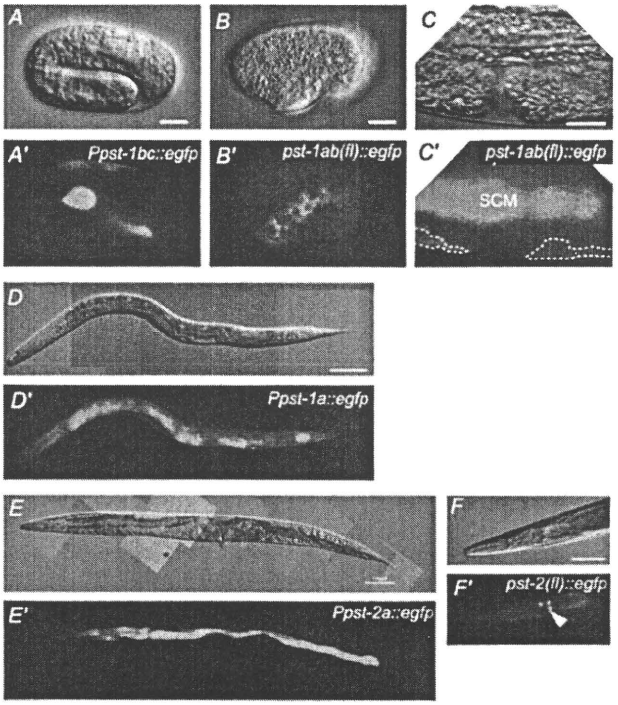

FIGURE 6. **Expression patterns of *pst-1* and *pst-2* reporter constructs in wild-type animals.** Transgene reporter analyses of *pst-1* (*A–D*) and *pst-2* (*E* and *F*). DIC (*A–F*) and fluorescent (*A'–F'*) images are shown. GFP was visualized directly under a fluorescence microscope except in *B'* and *C'*, which were sliced samples immunostained with an anti-GFP antibody. *A* and *A'*, expression pattern of $P_{pst\text{-}1bc}$::*egfp* in a folded embryo. EGFP is dominantly expressed in seam cells. *B*, *B'*, *C*, and *C'*, expression pattern of *pst-1ab(fl)*::*egfp* in an embryo (*B*) and the mid-ventral region (*C*) of a mid-L4 hermaphrodite. EGFP is dominantly expressed in seam cells. EGFP is expressed in seam cells (*SCM*) and the hypodermis (indicated with *dashed lines*) but not in the vulva (*C'*). *D* and *D'*, expression pattern of $P_{pst\text{-}1a}$::*egfp* in a mid-L4 larva. EGFP is expressed in almost all cells. *E* and *E'*, expression pattern of $P_{pst\text{-}2a}$::*egfp* in a young adult animal. EGFP is expressed in the intestine and pharyngeal gland cells. GFP expression in pharyngeal gland cells is weaker than in the intestine in this animal. *F* and *F'*, expression pattern of *pst-2(fl)*::*egfp* in the head region of a young adult animal. The EGFP signal in the pharyngeal gland cells is indicated with an *arrowhead*. *Scale bars* = 10 μm (*A–C*) and 100 μm (*E–F*).

$P_{pst\text{-}1bc}$::*egfp* vectors, GFP fluorescence was specifically observed in seam cells and amphid sheath cells during embryonic and larval development (Fig. 6, *A* and *B*). GFP expression was also detected in the hypodermis of L4 transgenic animals that carried *pst-1ab(fl)*::*egfp* (Fig. 6*C*) and *pst-1c(fl)*::*egfp*. Although the *pst-1* mutant displayed a vulval defect, no vulval expression was observed in these transgenic worms (Fig. 6*C*). In contrast, in transgenic animals that carried $P_{pst\text{-}1a}$::*egfp*, GFP fluorescence was observed in almost all cells throughout development except germ cells, where extrachromosomal transgenes are generally silenced (Fig. 6*D*). The *pst-1ab(fl)*::*egfp* and *pst-1c(fl)*::*egfp* constructs included the entire sequence of *pst-1a*, but $P_{pst\text{-}1a}$::*egfp* carried only the 5′-promoter region of *pst-1a*. Thus, broad expression of $P_{pst\text{-}1a}$::*egfp* might be induced due to the absence of a regulatory region for transgene expression. Additionally, the expression pattern induced by a promoter of the M03F8.3 gene, a gene immediately upstream of *pst-1*, was similar to that induced by the *pst-1a* promoter (sEx10297 transgene). Expression data from a genome-wide *in situ* hybridization analysis indicated that *pst-1* mRNA was specifically expressed in lateral seam cells, the adult germ line, and early embryos (a cDNA group, CELK04198, NextDB (nematode expression pattern database)).

In transgenic animals that carried the $P_{pst\text{-}2a}$::*egfp* and *pst-2(fl)*::*egfp* constructs, EGFP fluorescence was specifically observed in intestinal and pharyngeal gland cells (Fig. 6, *E* and *F*). However, no GFP signal was observed in worms carrying $P_{pst\text{-}2b}$::*egfp* (data not shown). This suggested that the *pst-2b*

promoter does not have inherent activity. Although there are no expression data for *pst-2* in the NextDB, *pst-2* is among the set of 603 germ line-specific/enriched genes identified by SAGE (serial analysis of gene expression). In the SAGE library, we found 10 tags for *pst-2* in the germ line and four tags in the soma, suggesting that *pst-2* is expressed predominantly in the germ line (64). Taken together, these results suggest that although both *pst-1* and *pst-2* are likely to be expressed in the germ line, they have mutually exclusive expression patterns in somatic cells; *pst-1* tends to be dominantly expressed in tissues generated from ectodermal cells, and *pst-2* tends to be expressed in tissues generated from endomesodermal cells.

PST-1 and PST-2 Are Localized to the Golgi Apparatus—In cultured mammalian cells, PAPS transporters have been shown to localize to the Golgi membrane (20, 25, 26). Our reporter analyses indicated that *pst-1* and *pst-2* are expressed in the hypodermis and intestine, respectively. Thus, we examined the subcellular localizations of PST-1·EGFP and PST-2·EGFP in those tissues. Consistent with the previous reports, the transporter proteins PST-1·EGFP and PST-2·EGFP co-localized with a marker of the Golgi apparatus, mCherry-tagged alpha-mannosidase II (AMAN-2). This suggested that PST-1 and PST-2 proteins reside in the Golgi (supplemental Fig. S4, *A* and *B*). However, in merged images, it was apparent that although PST-2·EGFP almost completely co-localized with AMAN-2, PST-1·EGFP only partly co-localized with AMAN-2 (supplemental Fig. S4*C*). The localization of AMAN-2 is predicted to be in the cis/medial-Golgi compartments rather than the trans-Golgi compartment. Thus, our results suggested that PST-2, but not PST-1, was distributed primarily in the cis/medial-Golgi compartments.

PST-1 Expression in the Epidermis Is Sufficient for Proper Larval Epithelial Development, and Its Expression in the Neuroectoblast Is Sufficient for Rescuing Embryonic Lethality—To determine which cell types required *pst-1* gene function, we examined whether epidermal, neuronal, or muscle expression of *pst-1* was sufficient to rescue the embryonic, vulval, and cuticle phenotypes of deletion mutants. Epidermis-specific expression of *pst-1b::egfp* under the control of the *dpy-7* promoter rescued vulval and abnormal cuticle phenotypes (Figs. 3*E* and 4*B*) and exhibited weak activity, but it was sufficient to rescue the embryonic phenotype (Table 4). The neuroectoderm- and neuron-specific expression of *pst-1b::egfp* under the control of the *unc-119* promoter only partially rescued vulval and abnormal cuticle phenotypes (Figs. 3*E* and 4*B*). However, it rescued the embryonic lethal phenotype more completely than epidermis-specific expression (Table 4). In contrast, differentiated neuron-specific or body wall muscle-specific expression of *pst-1b::egfp* under the control of *rgef-1* or *myo-3* promoters did not rescue any of the phenotypes. These results suggested that *pst-1* has specific functions in epidermal tissues during larval development and in epidermal precursors and/or neuroblasts during embryogenesis.

pst-2 Synergizes with pst-1 in Cuticle Formation but Not in Vulval Development or Embryogenesis—To investigate the genetic relationship between *pst-1* and *pst-2*, we examined the *pst-1;pst-2* double mutant phenotypes. The *pst-1* mutants exhibited abnormalities in embryogenesis, vulval development, and cuticle formation, but the *pst-2* mutants displayed essentially normal phenotypes (Figs. 3*E* and 4*B*). These data suggested that *pst-1* and *pst-2* do not have redundant roles in embryogenesis and vulval development. In contrast, the alkaline bleach sensitivity test revealed that the *pst-1;pst-2* double mutant had a more severely fragile cuticle than the *pst-1* single mutant (Fig. 3*E*), despite their similarities in DIC analyses. This suggested that *pst-1* and *pst-2* had some redundant functions in cuticle formation. To determine whether the redundancy between *pst-1* and *pst-2* resulted from the molecular function of the PAPS transporter, we ectopically expressed *pst-2* in the epidermis of the *pst-1(tm3364)* mutant and examined the effect on cuticle abnormality. The alkaline bleach sensitivity test revealed that *pst-2* expressed in the epidermis under control of the *dpy-7* promoter failed to rescue cuticle fragility in *pst-1(tm3364)* mutants; in contrast, *pst-1b* expression successfully rescued cuticle fragility (Fig. 3*E*). These results suggested that PST-1 and PST-2 play differential physiological roles in cuticle formation.

TABLE 4
Either neuroectodermal or epidermal expression of PST-1 was necessary and sufficient for embryogenesis

Promoter	Target tissue	No. of plates with proliferating progeny/ total test plates[a]	Rescue activity[b]
		10 larvae/plate	
None		0/2	−
pst-1bc	Hypodermis, seam cells, amphid sheath	2/2, 2/2[c]	++
dpy-7	Hypodermis, seam cells	3/5, 3/3[c]	+
unc-119	Neuroectoderm, differentiated neurons	2/2, 2/2[c]	++
rgef-1	Differentiated neurons	0/3	−
myo-3	Body wall muscles	0/3	−

[a] Ten L4 larvae of mutant or transgenic animals were transferred to a fresh plate seeded with OP50 to determine whether the animals could proliferate after 1 week.
[b] Lethality in transgenic *pst-1(tm3364)* mutant embryos that carried P_{dpy-7}*::pst-1b::egfp* was higher than in those that carried $P_{unc-119}$*:pst-1b::egfp* or *pst-1bc(fl)::egfp*.
[c] Two independent transgenic lines were tested.

DISCUSSION

This study showed that, in *C. elegans*, the PAPS transporter *pst-1* gene, but not the *pst-2* gene, is essential for diverse aspects of epithelial development, somatic gonadal cell migration, and viability. We observed embryonic defects in *pst-1* knock-out worms similar to those observed in embryos deficient in *pps-1* (15) or *rib-1/rib-2*, which lacked HS-synthesizing enzymes (41, 62). During larval development, the *pst-1* mutant showed defective cuticle formation similar to that observed in larvae depleted of *pps-1* or tyrosylprotein sulfotransferase-A (*tpst-1*) genes (15, 37). Although disaccharide analysis revealed that both *pst-1* and *pst-2* were involved in HS sulfation, none of the defects caused by the *pst-1* mutation could be restored by the heterogeneous expression of hPAPST2 or PST-2. Moreover, HS sulfation patterns isolated from *pst-1* mutant animals were clearly different from those isolated from *pst-2* mutant animals. Furthermore, *pst-1* and *pst-2* displayed different expression patterns. These observations indicated that hPAPST1/PST-1 has distinct characteristics from hPAPST2/PST-2 *in vivo*. Our data also suggested that subcellular localization of the PST-

1·EGFP protein was slightly different from that of the PST-2·EGFP protein. Thus, each PAPS transporter may reside in different intracellular compartments; this would allow differential sulfation reactions within a single cell. Intriguingly, differential "Golgi units" are proposed to regulate different glycosylation reactions in *Drosophila* cells (65).

Analysis using the yeast heterologous system clearly suggested that PST-1 and PST-2 are PAPS-specific transporters. Although PST-2 showed weaker transport activity compared with PST-1, the transporter activity in our assay was statistically significant, and PST-2 showed no transport activity for nucleotide sugars. These results together with the reduced sulfation in the *pst-2* null allele HS disaccharide analysis strongly indicate that PST-2 is also a PAPS transporter. It is intriguing that the total amount of HS disaccharide units was decreased in *pst-2* mutant but not in the *pst-1* null allele. Because sulfation takes place simultaneously with elongation of the GAG chain (66), depletion of PAPS in the intracellular compartment containing PST-2 may specifically influence the synthesis of GAG chains and reduce the heparan sulfate content measured in *pst-2* null mutant animals.

The *pst-1*, *pst-2* double mutant showed that PST-1 and PST-2 had synergistic effects in cuticle formation. Precise cuticle formation requires both epithelial cells and pharyngeal gland cells (67). Epithelial cells synthesize the cuticle, and pharyngeal gland cells are thought to secrete a surface coating that covers the cuticle. Our results showed that *pst-2* was expressed in pharyngeal gland cells, and thus in these cells, PST-2 may be involved in the secretion or synthesis of components of the cuticle surface coat. Another nucleotide sugar transporter, SRF-3, transports UDP-GlcNAc and UDP-Gal into Golgi apparatus-enriched vesicles from the cytosol. SRF-3 is expressed in pharyngeal gland cells and seam cells. It is involved in the biosynthesis of glycoconjugates for the outer surface and the cuticle (68, 69). Considering the expression patterns of PST-2, it is possible that PST-2 may cooperate with SRF-3 in this process. We also found that PST-2 was strongly expressed in the intestine, consistent with the tissue distribution of hPAPST2 transcripts (26). This implies that PST-2 and hPAPST2 may play a common role in the intestine; for example, they may participate in host-pathogen interactions.

Vulval morphogenesis, including invagination and final cell positioning along the anterior-posterior axis, was affected in *pst-1* mutant animals. Our data suggest that *pst-1* is required for the precise expression of *lin-11*::*gfp*. Similar findings have been reported for worms that expressed mutant *lin-17*, a gene that encodes the Frizzled Wnt receptor (46, 70, 71). HS proteoglycans are essential for Wnt signaling, both in vertebrates and invertebrates (72), and thus the sulfation of HS proteoglycans could modulate Wnt/Frizzled signaling or *lin-11* transcriptional regulation in vulval cells.

Immunostaining experiments have indicated that HS is present in vulval cells and around the vulva (Ref. 73 and our unpublished data). Consistent with this finding, abnormal vulval morphogenesis is thought to result from the loss of *rib-2* (a glucosaminyltransferase) function (74). Other glycosyltransferase genes (*sqv-6*, *sqv-2*, *sqv-8*, and *sqv-3*) involved in establishing proteoglycan linkages are required for synthesis of both HS and chondroitin. Mutations of *sqv* genes cause the Sqv phenotype, which was also observed in the *pst-1* mutant. As ample evidence indicates that chondroitin is not sulfated in this organism (34–36), the Sqv phenotype in *pst-1* mutant would be due to undersulfation of HS rather than chondroitin. However, animals with mutations in the *sqv* genes do not exhibit abnormal anterior-posterior cell positioning or small ectopic invaginations (60), despite their requirement for HS synthesis. This apparent discrepancy might be ascribed to the different half-lives of the different gene products studied (mRNA or proteins) and/or to different metabolic functions of the enzymes studied (PAPS transport *versus* GAG linkage). Further study of these genes in the vulval development will provide useful information concerning the fundamental machinery of GAG synthesis and metabolism, as well as the regulation of extracellular signaling by GAGs.

Mutation of *pst-1* also resulted in abnormal EMS cell division and post-embryonic seam cell development, which are regulated by Wnt signaling (75). This gives rise to the intriguing possibility that sulfation of extracellular molecules could be involved in regulation of proteins associated with Wnt signaling in diverse processes in *C. elegans*.

The lethality observed in the *pst-1* mutants isolated in this study occurred at a different embryonic stage than that observed in the *pps-1* null mutant (*tm1109*) that we isolated previously (15). The animals with *pst-1* mutations survived through the embryonic stage of the second generation; in contrast, animals with *pps-1* mutations died in L2/L3 of the first generation. This difference in timing can be explained by several possibilities. (i) Cytosolic sulfation is essential for L2/L3 growth. To date, no null mutation of *ssu-1*, which encodes the only known *C. elegans* ortholog of cytosolic sulfotransferase, has been isolated (76–78). However, deficiencies in *ssu-1*, by RNA interference or reduction-of-function mutations, did not result in a lethal phenotype. (ii) Extracellular sulfation is essential for L2/L3 growth, and PST-1 may not be the only Golgi-resident PAPS transporter, or there may be a novel mechanism for providing PAPS to Golgi-resident sulfotransferases. (iii) Neither cytosolic nor extracellular sulfation is required for L2/L3 growth, and PPS-1 has a function distinct from PAPS synthesis *in vivo*. Understanding how lethality is caused by *pps-1* and *pst-1* deficiencies will shed light on the mechanisms that underlie the regulation of PAPS metabolism and sulfation in *C. elegans* development.

While this manuscript was in preparation, Bülow and colleagues (43) published a paper concentrating on the analysis of *pst-1* and *pst-2* functions in the nervous system of *C. elegans*. They show that *pst-1* is essential in nervous system development and other functions, and our results are complementary to their results indicating the essentiality of PAPS transporters in the organism.

Acknowledgments—We thank Dr. K. Fukushima and Prof. K. Yamashita (Tokyo Institute of Technology, Yokohama, Japan) for providing the mammalian total cDNA. We also thank the Caenorhabditis Genetics Center, which is funded by the National Institutes of Health, NCRR, for the worms and E. coli strains. We also thank Adam Kleinschmit for useful comments.

REFERENCES

1. Kehoe, J. W., and Bertozzi, C. R. (2000) *Chem. Biol.* **7,** R57–R61
2. Schwartz, N. B., and Domowicz, M. (2002) *Glycobiology* **12,** 57R–68R
3. Honke, K., Zhang, Y., Cheng, X., Kotani, N., and Taniguchi, N. (2004) *Glycoconj. J.* **21,** 59–62
4. Zhang, H., Uchimura, K., and Kadomatsu, K. (2006) *Ann. N.Y. Acad. Sci.* **1086,** 81–90
5. Bishop, J. R., Schuksz, M., and Esko, J. D. (2007) *Nature* **446,** 1030–1037
6. Sugahara, K., and Mikami, T. (2007) *Curr. Opin. Struct. Biol.* **17,** 536–545
7. Nadanaka, S., and Kitagawa, H. (2008) *J. Biochem.* **144,** 7–14
8. Morita, I., Kizuka, Y., Kakuda, S., and Oka, S. (2008) *J. Biochem.* **143,** 719–724
9. Robbins, P. W., and Lipmann, F. (1957) *J. Biol. Chem.* **229,** 837–851
10. Klaassen, C. D., and Boles, J. W. (1997) *FASEB J.* **11,** 404–418
11. Strott, C. A. (2002) *Endocr. Rev.* **23,** 703–732
12. Robbins, P. W., and Lipmann, F. (1958) *J. Biol. Chem.* **233,** 681–685
13. Zaruba, M. E., Schwartz, N. B., and Tennekoon, G. I. (1988) *Biochem. Biophys. Res. Commun.* **155,** 1271–1277
14. Besset, S., Vincourt, J. B., Amalric, F., and Girard, J. P. (2000) *FASEB J.* **14,** 345–354
15. Dejima, K., Seko, A., Yamashita, K., Gengyo-Ando, K., Mitani, S., Izumikawa, T., Kitagawa, H., Sugahara, K., Mizuguchi, S., and Nomura, K. (2006) *J. Biol. Chem.* **281,** 11431–11440
16. Schwarz, J. K., Capasso, J. M., and Hirschberg, C. B. (1984) *J. Biol. Chem.* **259,** 3554–3559
17. Carlsson, P., Presto, J., Spillmann, D., Lindahl, U., and Kjellén, L. (2008) *J. Biol. Chem.* **283,** 20008–20014
18. Sohaskey, M. L., Yu, J., Diaz, M. A., Plaas, A. H., and Harland, R. M. (2008) *Development* **135,** 2215–2220
19. Frederick, J. P., Tafari, A. T., Wu, S. M., Megosh, L. C., Chiou, S. T., Irving, R. P., and York, J. D. (2008) *Proc. Natl. Acad. Sci. U.S.A.* **105,** 11605–11612
20. Dick, G., Grøndahl, F., and Prydz, K. (2008) *Glycobiology* **18,** 53–65
21. Capasso, J. M., and Hirschberg, C. B. (1984) *Proc. Natl. Acad. Sci. U.S.A.* **81,** 7051–7055
22. Mandon, E. C., Milla, M. E., Kempner, E., and Hirschberg, C. B. (1994) *Proc. Natl. Acad. Sci. U.S.A.* **91,** 10707–10711
23. Ozeran, J. D., Westley, J., and Schwartz, N. B. (1996) *Biochemistry* **35,** 3695–3703
24. Ozeran, J. D., Westley, J., and Schwartz, N. B. (1996) *Biochemistry* **35,** 3685–3694
25. Kamiyama, S., Suda, T., Ueda, R., Suzuki, M., Okubo, R., Kikuchi, N., Chiba, Y., Goto, S., Toyoda, H., Saigo, K., Watanabe, M., Narimatsu, H., Jigami, Y., and Nishihara, S. (2003) *J. Biol. Chem.* **278,** 25958–25963
26. Kamiyama, S., Sasaki, N., Goda, E., Ui-Tei, K., Saigo, K., Narimatsu, H., Jigami, Y., Kannagi, R., Irimura, T., and Nishihara, S. (2006) *J. Biol. Chem.* **281,** 10945–10953
27. Goda, E., Kamiyama, S., Uno, T., Yoshida, H., Ueyama, M., Kinoshita-Toyoda, A., Toyoda, H., Ueda, R., and Nishihara, S. (2006) *J. Biol. Chem.* **281,** 28508–28517
28. Lüders, F., Segawa, H., Stein, D., Selva, E. M., Perrimon, N., Turco, S. J., and Häcker, U. (2003) *EMBO J.* **22,** 3635–3644
29. Ali, R. A., Mellenthin, K., Fahmy, K., Da Rocha, S., and Baumgartner, S. (2005) *Dev. Genes. Evol.* **215,** 537–543
30. Clément, A., Wiweger, M., von der Hardt, S., Rusch, M. A., Selleck, S. B., Chien, C. B., and Roehl, H. H. (2008) *PLoS Genet.* **4,** e1000136
31. Sherman, T., Chernova, M. N., Clark, J. S., Jiang, L., Alper, S. L., and Nehrke, K. (2005) *Am. J. Physiol. Cell Physiol.* **289,** C341–C351
32. Bülow, H. E., and Hobert, O. (2004) *Neuron* **41,** 723–736
33. Mizuguchi, S., and Dejima, D., and Nomura, K. (2009) *Trends Glycosci. Glycotechnol.* **21,** 179–191
34. Yamada, S., Van Die, I., Van den Eijnden, D. H., Yokota, A., Kitagawa, H., and Sugahara, K. (1999) *FEBS Lett.* **459,** 327–331
35. Toyoda, H., Kinoshita-Toyoda, A., and Selleck, S. B. (2000) *J. Biol. Chem.* **275,** 2269–2275
36. Nabetani, T., Miyazaki, K., Tabuse, Y., and Tsugita, A. (2006) *Proteomics* **6,** 4456–4465
37. Kim, T. H., Hwang, S. B., Jeong, P. Y., Lee, J., and Cho, J. W. (2005) *FEBS Lett.* **579,** 53–58
38. Berninsone, P. M. (December 18, 2006) in *WormBook* (*C. elegans* Research Community, ed) doi/10.1895/wormbook.1.125.1, http://www.wormbook.org
39. Gumienny, T. L., MacNeil, L. T., Wang, H., de Bono, M., Wrana, J. L., and Padgett, R. W. (2007) *Curr. Biol.* **17,** 159–164
40. Franks, D. M., Izumikawa, T., Kitagawa, H., Sugahara, K., and Okkema, P. G. (2006) *Dev. Biol.* **296,** 409–420
41. Kitagawa, H., Izumikawa, T., Mizuguchi, S., Dejima, K., Nomura, K. H., Egusa, N., Taniguchi, F., Tamura, J., Gengyo-Ando, K., Mitani, S., Nomura, K., and Sugahara, K. (2007) *J. Biol. Chem.* **282,** 8533–8544
42. Bülow, H. E., Tjoe, N., Townley, R. A., Didiano, D., van Kuppevelt, T. H., and Hobert, O. (2008) *Curr. Biol.* **18,** 1978–1985
43. Bhattacharya, R., Townley, R. A., Berry, K. L., and Bülow, H. E. (2009) *J. Cell Sci.* **122,** 4492–4504
44. Brenner, S. (1974) *Genetics* **77,** 71–94
45. Burdine, R. D., Branda, C. S., and Stern, M. J. (1998) *Development* **125,** 1083–1093
46. Gupta, B. P., and Sternberg, P. W. (2002) *Dev. Biol.* **247,** 102–115
47. Mohler, W. A., Simske, J. S., Williams-Masson, E. M., Hardin, J. D., and White, J. G. (1998) *Curr. Biol.* **8,** 1087–1090
48. Gengyo-Ando, K., and Mitani, S. (2000) *Biochem. Biophys. Res. Commun.* **269,** 64–69
49. Mizuguchi, S., Uyama, T., Kitagawa, H., Nomura, K. H., Dejima, K., Gengyo-Ando, K., Mitani, S., Sugahara, K., and Nomura, K. (2003) *Nature* **423,** 443–448
50. Izumikawa, T., Kitagawa, H., Mizuguchi, S., Nomura, K. H., Nomura, K., Tamura, J., Gengyo-Ando, K., Mitani, S., and Sugahara, K. (2004) *J. Biol. Chem.* **279,** 53755–53761
51. Kinoshita, A., and Sugahara, K. (1999) *Anal. Biochem.* **269,** 367–378
52. Gravato-Nobre, M. J., Nicholas, H. R., Nijland, R., O'Rourke, D., Whittington, D. E., Yook, K. J., and Hodgkin, J. (2005) *Genetics* **171,** 1033–1045
53. Gengyo-Ando, K., Yoshina, S., Inoue, H., and Mitani, S. (2006) *Biochem. Biophys. Res. Commun.* **349,** 1345–1350
54. Dejima, K., Murata, D., Mizuguchi, S., Nomura, K. H., Gengyo-Ando, K., Mitani, S., Kamiyama, S., Nishihara, S., and Nomura, K. (2009) *FASEB J.* **23,** 2215–2225
55. Gilleard, J. S., Barry, J. D., and Johnstone, I. L. (1997) *Mol. Cell. Biol.* **17,** 2301–2311
56. Mello, C., and Fire, A. (1995) *Methods Cell Biol.* **48,** 451–482
57. Miller, D. M., and Shakes, D. C. (1995) *Methods Cell Biol.* **48,** 365–394
58. Käll, L., Krogh, A., and Sonnhammer, E. L. (2005) *Bioinformatics* **21,** Suppl. 1, i251–i257
59. Käll, L., Krogh, A., and Sonnhammer, E. L. (2007) *Nucleic Acids Res.* **35,** W429-W432
60. Herman, T., Hartwieg, E., and Horvitz, H. R. (1999) *Proc. Natl. Acad. Sci. U.S.A.* **96,** 968–973
61. Hwang, H. Y., Olson, S. K., Esko, J. D., and Horvitz, H. R. (2003) *Nature* **423,** 439–443
62. Morio, H., Honda, Y., Toyoda, H., Nakajima, M., Kurosawa, H., and Shirasawa, T. (2003) *Biochem. Biophys. Res. Commun.* **301,** 317–323
63. Chisholm, A. D., and Hardin, J. (December 01, 2005) in *WormBook* (*C. elegans* Research Community, ed) doi/10.1895/wormbook.1.35.1, http://www.wormbook.org
64. Wang, X., Zhao, Y., Wong, K., Ehlers, P., Kohara, Y., Jones, S. J., Marra, M. A., Holt, R. A., Moerman, D. G., and Hansen, D. (2009) *BMC Genomics* **10,** 213
65. Yano, H., Yamamoto-Hino, M., Abe, M., Kuwahara, R., Haraguchi, S., Kusaka, I., Awano, W., Kinoshita-Toyoda, A., Toyoda, H., and Goto, S. (2005) *Proc. Natl. Acad. Sci. U.S.A.* **102,** 13467–13472
66. Silbert, J. E., and Sugumaran, G. (1995) *Biochim. Biophys. Acta* **1241,** 371–384
67. Nelson, F. K., Albert, P. S., and Riddle, D. L. (1983) *J. Ultrastruct. Res.* **82,** 156–171
68. Höflich, J., Berninsone, P., Göbel, C., Gravato-Nobre, M. J., Libby, B. J., Darby, C., Politz, S. M., Hodgkin, J., Hirschberg, C. B., and Baumeister, R. (2004) *J. Biol. Chem.* **279,** 30440–30448

69. Cipollo, J. F., Awad, A. M., Costello, C. E., and Hirschberg, C. B. (2004) *J. Biol. Chem.* **279,** 52893–52903
70. Sternberg, P. W., and Horvitz, H. R. (1988) *Dev. Biol.* **130,** 67–73
71. Sawa, H., Lobel, L., and Horvitz, H. R. (1996) *Genes Dev.* **10,** 2189–2197
72. Lin, X. (2004) *Development* **131,** 6009–6021
73. Minniti, A. N., Labarca, M., Hurtado, C., and Brandan, E. (2004) *J. Cell Sci.* **117,** 5179–5190
74. Bender, A. M., Kirienko, N. V., Olson, S. K., Esko, J. D., and Fay, D. S. (2007) *Dev. Biol.* **302,** 448–462
75. Eisenmann, D. M. (June 25, 2005) in *WormBook* (*C. elegans* Research Community, ed) doi/10.1895/wormbook.1.7.1, http://www.wormbook.org
76. Carroll, B. T., Dubyak, G. R., Sedensky, M. M., and Morgan, P. G. (2006) *J. Biol. Chem.* **281,** 35989–35996
77. Hattori, K., Inoue, M., Inoue, T., Arai, H., and Tamura, H. O. (2006) *J. Biochem.* **139,** 355–362
78. Sönnichsen, B., Koski, L. B., Walsh, A., Marschall, P., Neumann, B., Brehm, M., Alleaume, A. M., Artelt, J., Bettencourt, P., Cassin, E., Hewitson, M., Holz, C., Khan, M., Lazik, S., Martin, C., Nitzsche, B., Ruer, M., Stamford, J., Winzi, M., Heinkel, R., Röder, M., Finell, J., Häntsch, H., Jones, S. J., Jones, M., Piano, F., Gunsalus, K. C., Oegema, K., Gönczy, P., Coulson, A., Hyman, A. A., and Echeverri, C. J. (2005) *Nature* **434,** 462–469

BJ www.biochemj.org

BJ Disease

Biochem. J. (2010) **432**, 47–55 (Printed in Great Britain) doi:10.1042/BJ20100847

Chondroitin sulfate N-acetylgalactosaminyltransferase-1 is required for normal cartilage development

Yumi WATANABE*†[1], Kosei TAKEUCHI*†[1], Susumu HIGA ONAGA*[1], Michiko SATO*, Mika TSUJITA†, Manabu ABE‡, Rie NATSUME‡, Minqi LI†§, Tatsuya FURUICHI‖[2], Mika SAEKI¶, Tomomi IZUMIKAWA¶, Ayumi HASEGAWA**, Minesuke YOKOYAMA**, Shiro IKEGAWA‖, Kenji SAKIMURA‡, Norio AMIZUKA†§, Hiroshi KITAGAWA¶ and Michihiro IGARASHI*†[3]

*Division of Molecular and Cellular Biology, Graduate School of Medical and Dental Sciences, Niigata University, 1–757 Asahi-machi, Chuo-ku, Niigata 951-8510, Japan, †Trans-disciplinary Research Program, Niigata University, Niigata 951-8510, Japan, ‡Department of Cellular Neurobiology, Niigata University, Niigata 951-8510, Japan, §Department of Developmental Biology of Hard Tissue, Division of Oral Health Science, Hokkaido University Graduate School of Dental Medicine, Kita 13, Nishi 7, Kita-ku, Sapporo 060-8586, Japan, ‖Laboratory for Bone and Joint Diseases, Center for Genome Medicine, RIKEN, 4-6-1 Shirokanedai Minato-ku, Tokyo 108-8639, Japan, ¶Department of Biochemistry, Kobe Pharmaceutical University, Higashinada-ku, Kobe 658-8558, Japan, and **Department of Comparative and Experimental Medicine, Brain Research Institute, Niigata University, Niigata 951-8510, Japan

CS (chondroitin sulfate) is a glycosaminoglycan species that is widely distributed in the extracellular matrix. To understand the physiological roles of enzymes involved in CS synthesis, we produced *CSGalNAcT1* (CS N-acetylgalactosaminyltransferase 1)-null mice. CS production was reduced by approximately half in *CSGalNAcT1*-null mice, and the amount of short-chain CS was also reduced. Moreover, the cartilage of the null mice was significantly smaller than that of wild-type mice. Additionally, type-II collagen fibres in developing cartilage were abnormally aggregated and disarranged in the homozygous mutant mice. These results suggest that CSGalNAcT1 is required for normal CS production in developing cartilage.

Key words: cartilage, chondroitin sulfate, collagen fibre, N-acetylgalactosaminyltransferase (GalNAcT), gene knockout, glycosaminoglycan.

INTRODUCTION

CS (chondroitin sulfate) is a type of GAG (glycosaminoglycan), which are present in the extracellular matrices and on the surface of many cell types [1]. Similar to other GAGs, CS is attached to a serine residue of the core protein to form the CSPG [CS PG (proteoglycan)] [1]. After the formation of a common linkage region (GlcUAβ1-3Galβ1-3Galβ1-4Xylβ1-*O*-Ser) between sugar chains and the core protein, repeating disaccharide units of GalNAc (*N*-acetylgalactosamine) and GlcUA (glucuronic acid) residues with interspersed sulfate residues are synthesized [1]. Thus biosynthesis of a CS-specific polysaccharide chain is initiated by the transfer of a GalNAc residue to the tetrasaccharide linker, followed by the addition of GlcUA and GalNAc residues in reiterative chain elongation steps.

There are six glycosyltransferases known to be involved in CS synthesis [2–10]. Among them, CSGalNAcT1 (CS N-acetylgalactosaminyltransferase-1) and CSGalNAcT2 each have one glycosyltransferase domain, exhibit GalNAc transfer activity in both the initiation and elongation processes, and are thought to be responsible for the addition of the first GalNAc residue to the tetrasaccharide chain [4–7]. Although each of the six enzymes has been characterized biochemically in *in vitro* studies, the mechanism of *in vivo* CS biosynthesis, including roles for each glycosyltransferase, is poorly understood. Since cartilage contains the largest amount of CS of all body tissues, chondrocytes efficiently synthesize CS chains [11,12]. CS in cartilage is selectively linked to aggrecan, which can possess more than 100 CS chains; these CSPGs subsequently form multimolecular aggregates through interaction with hyaluronate and linker proteins [13]. CSGalNAcT1 is highly expressed in the developing cartilage, and this enzyme is thought to play a crucial role in CS biosynthesis on the basis of a study using cell lines [14]. Moreover, CSGalNAcT1 is thought to have important roles in chondrogenesis at early developmental stages [14].

To investigate the physiological role of CSGalNAcT1 in CS biosynthesis, we produced *CSGalNAcT1*-null mice and analysed the morphology and biochemistry of developing cartilage in these mutants. The mice were viable and fertile; however, the amount of CS was reduced by half relative to the amount in wild-type controls, and the null mice showed an abnormal profile of GAG chains in the biochemical analysis of CS. The thickness of the epiphyseal cartilage layer was decreased by 25 % at E (embryonic day) 18.5. Moreover, the hindlimb and the body were also shorter. Taken together, our data suggest that CSGalNAcT1 plays a role in CS synthesis in the cartilage during embryonic development.

EXPERIMENTAL

Materials

Proteus vulgaris chondroitinase ABC (EC 4.2.2.4) was purchased from Seikagaku. The Superdex™ 200 10/300 GL column was obtained from Amersham Pharmacia Biotech.

Abbreviations used: 2-AB, 2-aminobenzamide; C4st-1, chondrotin 4-sulfotransferase-1; ChPF, chondroitin polymerization factor; ChSy, chondroitin synthase; CS, chondroitin sulfate; CSGalNAcT, chondroitin sulfate N-acetylgalactosaminyltransferase; CSPG, chondroitin sulfate proteoglycan; E, embryonic day; ES, embryonic stem; Fam20b, family member 20B; G3pdh, glyceraldehyde-3-phosphate dehydrogenase; GAG, glycosaminoglycan; GlcUA, glucuronic acid; HRP, horseradish peroxidase; PCNA, proliferating cell nuclear antigen; PG, proteoglycan; RT, reverse transcription; TEM, transmission electron microscope.

[1] These three authors contributed equally.

[2] Present address: Laboratory Animal Facility, Research Center for Medical Sciences, Jikei University School of Medicine, 3-25-8 Nishi-shinbashi, Minato-ku, Kobe 658-8558, Japan.

[3] To whom correspondence should be addressed (email tarokaja@med.niigata-u.ac.jp).

Generation of *CSGalNAcT1*-null mice

All animal experiments were carried out in accordance with the guidelines laid down by the animal welfare committees of Niigata University. The *CSGalNAcT1*-null mice were produced by homologous recombination using a new ES (embryonic stem) cell line, RENKA, which we developed from the *C57BL/6N* strain [15].

The mouse *CSGalNAcT1* gene (chondroitin 4-sulfotransferase-1) was identified by homology with the human *CSGalNAcT1* gene (GenBank® accesion number NM_172753) [encoding 530 amino acids; 89 % identity and 92 % similarity to human EC 2.4.1.174 (NM_001130518)]. A 1.8-kb DNA fragment, which carried the 34-bp loxP sequence and Pgk-1 promoter-driven neomycin phosphotransferase gene (neo) flanked by two Flp recognition target (frt) sites [16], was inserted into a site 372 bp upstream of exon 7. The 34-bp loxP sequence was inserted into a site 249 bp downstream of exon 6. The targeting vector, ptv *CSGALNACT1*-flox, contained exon 7 of the *CSGalNAcT1* gene flanked by loxP sequences, genomic sequences from 3.4 kb upstream and 7.1 kb downstream of exon 6, and a 4.3 kb pMC1DTpA vector [17].

ES cells were cultured on mitomycin C-treated neomycin-resistant fibroblasts in DMEM (Dulbecco's modified Eagle's medium; high glucose; Invitrogen) supplemented with 17.7 % ES-cell-qualified fetal bovine serum (Invitrogen), 88.4 μM non-essential amino acids (Invitrogen), 884 μM sodium pyruvate (Sigma), 88.4 μM 2-mercaptoethanol (Sigma) and 884 units/ml of murine leukaemia inhibitory factor (ESGRO; Chemicon International). Linearized targeting vector was electroporated into RENKA cells, and G-418 (175 μg/ml)-resistant clones were picked. Recombinant clones were identified by Southern blot hybridization analysis. Recombinant ES cells were injected into eight-cell-stage embryos of the CD-1 mouse strain. The embryos were cultured to blastocysts and transferred to the uterus of a pseudopregnant CD-1 mouse. Resulting chimaeric mice were mated to C57BL/6N mice, and heterozygous offspring [$CSGalNAcT1^{+/floxneo}$] were mated to telencephalin-*cre* mice [18,19]. The resulting heterozygous ($CSGalNAcT1^{+/-}$; $Cre^{+/-}$) mice were mated with C57BL/6N mice and the mice without the *Cre* gene were selected. Homozygous mutant mice and control mice were obtained by crossing heterozygous pairs.

Genotypes of the $CSGalNAcT1^{+/floxneo}$ mice and $CSGalNAcT1^{-/-}$ mice were identified by Southern blot hybridization analysis. Elimination of the *Cre* gene was confirmed by PCR using 5′-GCCTGCATTACCGGTCGATGCAACG-3′ (CreP1) and 5′-GCCCGGACCGACGATGAAGCATGTT-3′ (CreP2) [20] with internal control primers 5′-CCAGCTCCAGGGATCTAACA-3′ and 5′-ATTAAGGGCCAGCTCATTCC-3′ (glutamate receptor GluN2A subunit). Routine genotyping of $CSGalNAcT1^{+/-}$ animals was conducted by PCR using the primers 5′-CCAGCTCCAGGGATCTAACA-3′ and 5′-TGGTTTCCTCTAGCCATTGC-3′.

Derivatization of CS from articular cartilage using a fluorophore, 2-AB (2-aminobenzamide)

Articular cartilage CSPG from E18.5 embryos was extracted with 4 M guanidinium chloride and 0.05 M Tris/HCl, pH 8.0, containing proteinase inhibitors as described [21]. The extract was centrifuged at 15000 ***g*** for 10 min to remove insoluble material. The protein concentration of each sample was determined using a BCA (bicinchoninic acid) protein assay kit (Thermo Fisher Scientific) according to the manufacturer's instructions. The CSPG fractions were precipitated with 70 % ethanol containing 5 % sodium acetate. The partially purified CSPG fraction was digested with chondroitinase ABC, and the digests were then derivatized with 2-AB and analysed by HPLC as previously described [22].

Gel-filtration chromatography of CS

To determine the chain length of CS, the purified CSPG fraction was subjected to reductive β-elimination using $NaBH_4$/NaOH, and then analysed by gel-filtration chromatography on a column (10 × 300 mm) of Superdex 200 eluted with 0.2 M ammonium bicarbonate at a flow rate of 0.4 ml/min. Fractions were collected at 3 min intervals, lyophilized and digested with chondroitinase ABC. The digests were derivatized with 2-AB, and then analysed by HPLC on an amine-bound PA-03 column [22]. The amounts of the 2-AB derivatives of unsaturated disaccharides were calculated based on fluorescence intensity.

Quantitative real-time RT (reverse transcription)–PCR

Total RNA was extracted from articular cartilage using RNeasy Lipid Tissue Mini kit (Qiagen) according to the manufacturer's instructions. The cDNA was synthesized from ~1 μg of total RNA using Moloney-murine-leukaemia virus reverse transcriptase (Promega) and an oligo$(dT)_{20}$-M4 adaptor primer (Takara). The primer sequences used were as follows: *CSGalNAcT1*, forward primer 5′-CCAATTTCAGAAACTTCACCTTCAT-3′ and reverse primer 5′-TGTTCAGCCTACAAGTGTTGAG-3′; *CSGalNAcT2*, forward primer 5′-TTAATATCATTGTGCCACTTGCG-3′ and reverse primer 5′-TAGAATAGACTTGACTTTAGATAGTCCTT-3′; *C4st-1* (chondroitin 4-sulfotransferase-1), forward primer 5′-ACCTCGTGGGCAAGTATGAG-3′ and reverse primer 5′-TCTGGAAGAACTCCGTGGTC-3′; *Fam20B* (family member 20B) [23], forward primer 5′-TTGTCTTTAAGCCTAAGCGGT-3′ and reverse primer 5′-GGCTTAACTTCTGTCCGCA-3′; and *G3pdh* (glyceraldehyde-3-phosphate dehydrogenase), forward primer 5′-CATCTGAGGGCCCACTG-3′ and reverse primer 5′-GAGGCCATGTAGGCCATGA-3′. Quantitative real-time RT–PCR was performed using a FastStart DNA Master plus SYBR Green I (Roche Diagnostics) in a LightCycler ST300 (Roche Diagnostics). The expression levels of *CSGalNAcT1*, *CSGalNAcT2*, *C4st-1* and *Fab20B* mRNA were normalized to that of the *G3pdh* transcript.

Western blot analysis with anti-CSGalNAcT1 antibody

The anti-CSGalNAcT1 antibody was generated against recombinant GST (glutathione transferase)–CSGalNAcT1 (amino acids 261–534). E18.5 cartilage and brain extracts (0.1 mg of total protein) were subjected to SDS/PAGE (10 % gels), followed by immunoblot analysis.

Body length and weight

Measurements were performed on adults from the dorsal tip of the nose to the dorsal base of the tail while mice were under anaesthesia. The body weight and body length measurements were based on data from seven male offspring from seven unique litters. Statistical analysis was performed using a Student's *t* test and the data are represented as the means ± S.E.M. $*P < 0.05$.

Skeletal analysis

Embryos were eviscerated under anaesthetic (isoflurane or pentobarbital) and fixed in 100 % ethanol for 4 days. Toluidine Blue staining was performed in a solution of 80 % ethanol, 20 % acetic acid and 0.015 % Toluidine Blue for 4 days at

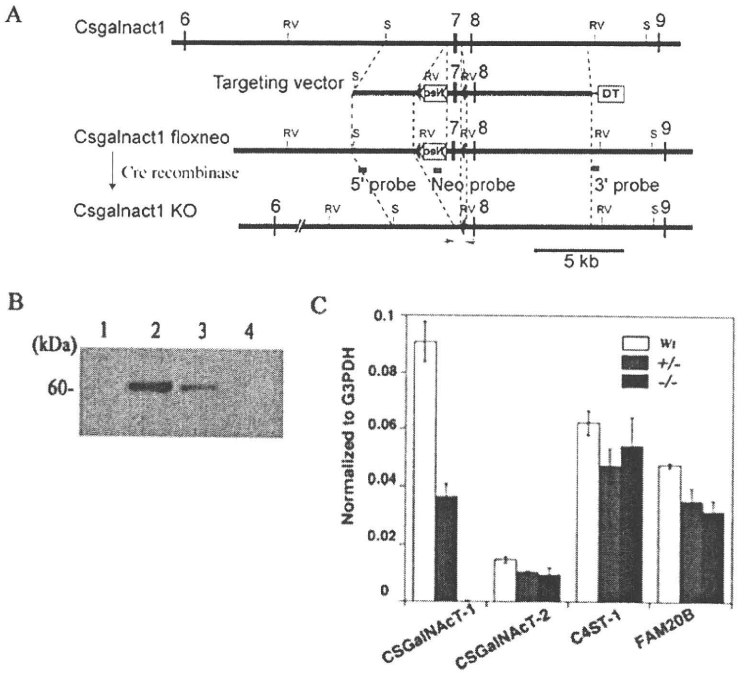

Figure 1 ***CSGalNAcT1*-null mice did not express the CSGalNAcT1 enzyme**

(**A**) Construct of the targeting vector for producing the *CSGalNAcT1*-null mice. The numbers represent the exon number (exon 1 is defined as the first exon of this gene where the transcription starts). RV, EcoRV site; S, ScaI site. (**B**) Immunoblot analysis using an anti-CSGalNAcT1 antibody to probe head homogenate from wild-type mice (lane 2), heterozygous (*CSGalNAcT1*$^{+/-}$) mice (lane 3) and null mice (*CSGalNAcT1*$^{-/-}$) at E18.5. Lane 1 shows the negative control (wild-type homogenate after absorption by the recombinant CSGalNAcT1 protein). Note that no reactivity was evident in the homogenate from null mice (lane 4). (**C**) RT–PCR analysis of genes encoding several enzymes involved in CS synthesis. The expression level is shown as a ratio of each gene to *G3pdh* for normalization. Fam20B is an enzyme that phosphorylates xylose [23]. Note that no other specific enzymes showed elevated expression to compensate for the loss of CSGalNAcT1 protein.

37 °C. Specimens were rinsed and soaked in 100 % ethanol for 3 days. Alizarin Red staining was then performed in a solution of 0.002 % Alizarin Red and 1 % KOH for 12 h at room temperature (25 °C). After rinsing with water, specimens were kept in 1 % KOH solution until the skeletons become clearly visible. For storage, specimens were transferred sequentially into 50 %, 80 %, and finally 100 % glycerol. Tibial length was determined by measuring the distance between the proximal and distal articular surfaces with a ruler under light microscopy.

Thickness of epiphyseal cartilage

To compare the thickness of epiphyseal cartilage of proximal femurs, formalin-fixed and paraffin-embedded bones of the limbs from E18.5 and at 4 weeks of postnatal development were used. The tissue material was sliced into serial sections and stained with haematoxylin/eosin. An SZX16 microscope (Olympus) with a digital camera Axiocam HRc (Zeiss) was used to collect image data from the serial sections, and the thickness of the epiphyseal cartilage was calculated from the length of the longitudinal centre axis by Imaris (Zeiss) and ImageJ (National Institutes of Health). A double-blind histological comparison between the null and the wild-type mice was performed. A Mann–Whitney *U* test was used to analyse the data.

Tissue preparation for mouse specimens

Mice were anaesthesitized with diethyl ether and pentobarbital (Nembutal; Dinabot) and then perfused with 4 % paraformaldehyde solution (pH 7.4) under anaethestia tibiae of E18.5 *CSGalNAcT1*$^{-/-}$ fetuses were extracted, decalcified, and embedded in paraffin as previously described [24]. Immunostained sections of the mice were observed under a Nikon Eclipse E800 microscope, and light microscopic images were acquired with a digital camera (Nikon DXM1200C). For TEM (transmission electron microscope) observations, fixed specimens were decalcified, post-fixed with osmium tetroxide, dehydrated, and embedded in epoxy resin (Epon 812) as previously described [10]. Ultra-thin sections were obtained with an ultra microtome (Sorvall MT-5000) and stained with an aqueous solution of 1 % tannic acid, 4 % uranyl acetate and 2 % lead citrate. These specimens were observed using a TEM (Hitachi H-7100) at 80 kV.

Immunostaining for type-II collagen and PCNA (proliferating cell nuclear antigen)

Dewaxed paraffin sections were pre-treated for endogenous peroxidase inhibition with 0.3 % H_2O_2 in PBS for 20 min and treated as described previously with a 0.5 % hyaluronidase solution (type I-S, from bovine testis; Sigma) for 10 min [24]. They were subjected to blocking for non-specific binding with BSA/PBS (1 % BSA in PBS) for 30 min at room temperature. Sections were then incubated with rabbit anti-type-II or type-X collagen (1:100; LSL) overnight at 4 °C followed by incubation with HRP (horseradish peroxidase)-conjugated anti-(rabbit Igs) (Chemicon International) overnight at 4 °C. Other sections were incubated with mouse monoclonal antibody against PCNA (Oncogene),

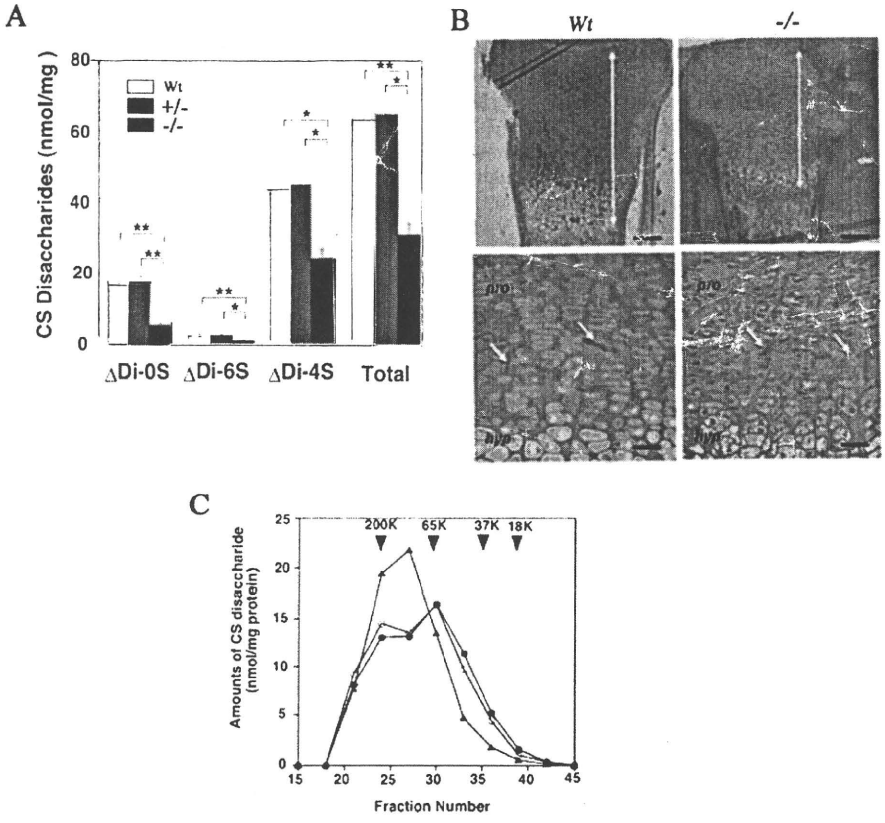

Figure 2 CS production in cartilage is reduced in *CSGalNAcT1*-null mice

(**A**) The total amount and disaccharide analysis of the cartilage in wild-type (Wt), heterozygous (+/−; *CSGalNAcT1*$^{+/-}$) and null (−/−; *CSGalNAcT1*$^{-/-}$) mice. Student's *t* test was performed to compare the disaccharide amount derived from CS in the null mice with that in the wild-type or the heterozygous mice. Results are shown as mean ± S.E.M. *$P < 0.05$; **$P < 0.01$ ($n = 6$). ΔDi-0S, ΔHexAα1-3GalNAc; ΔDi-4S, ΔHexAα1-3GalNAc(4S); ΔDi-6S, HexAα1-3GalNAc(6S). (**B**) Toluidine Blue staining of the epiphyseal cartilage from E18.5 wild-type (*Wt*; left) and *CSGalNAcT1*-null (−/−) fetuses. Metachromasia of Toluidine Blue (purple colour) can be seen in the wild-type cartilage, whereas no metachromasia is discernible in the null mice cartilage. Note the reduced size of the epiphyseal cartilage in the null mice, compared with their wild-type counterpart (bidirectional arrows, upper panels). The extracellular spaces in the cartilage of null mice have many spicules (arrows, lower panels), whereas the intercellular regions from wild-type mice do not. *pro*, proliferative zone; *hyp*, hypertrophic zone. Scale bars: in upper panels, 200 μm; in lower panels, 50 μm. (**C**) Gel-filtration analysis of the length of CS sugar chains in the E18.5 cartilage in wild-type (●), heterozygous (*CSGalNAcT1*$^{+/-}$; ○) and null (*CSGalNAcT1*$^{-/-}$; ▲) mice. There are no significant differences in the total amount of CS loaded on to the gels among groups. Note that the second peak between fraction numbers 30 and 35 is present both in wild-type and heterozygous mice, but not in *CSGalNAcT1*-null mice, indicating that the size of the GAG chains of CS changed in *CSGalNAcT1*-null mice. Arrowheads indicate the size of the molecular-mass-marker standards [mean molecular masses (K, kDa): 200, 65.5, 37.5 and 18.1 respectively, all from Sigma]. The calibration of the Superdex 200 column was performed using a series of size-defined commercial dextran polysaccharides. The results shown represent one of three series of independent experiments, where the three series of experiments gave essentially identical results.

followed by incubation with HRP-conjugated anti-(mouse IgG) (Chemicon). Visualization of the immune complex was performed with diaminobenzidine tetrahydrochloride. All sections were faintly counterstained with Methyl Green.

RESULTS

To investigate the role of CS synthesis in skeletal development, we inactivated the *CSGalNAcT1* gene by targeted gene replacement in ES cells and subsequent gene knockout in transgenic mice. The DXD motif is present in most GalNAc/Gal transferases and is essential to the *in vitro* activity of these enzymes as the binding site for divalent metal cations such as Mn^{2+} [25–27]; therefore we focused on this motif in our gene targeting and gene knockout strategy. Since mouse CSGalNAcT1 has a DXD motif that is encoded in exon 7, we designed the targeting vector with exon 7 located between two loxP sites. Specifically, the neomycin-resistance cassette (*neo*-cassette) was inserted adjacent to exon 7 (Figure 1A). After the *Cre* recombinase-dependent excision of the exonic sequences flanked by loxP sites, a frame shift occurs that should prevent the production of normal CSGalNAcT1 enzyme (Figure 1A).

The vector was introduced into the C57BL/6 ES cells, and chimaeric mice containing clonal recombinant ES cells were crossed with C57BL/6 mice. The complete null mice were obtained by mating the floxed mouse with a telencephalin-*Cre* mouse that expressed the *Cre*-recombinase in all cell types of early stage embryos (Figure 1A) [19].

The CSGalNAcT1 protein and *CSGalNAcT1* mRNA was completely absent from *CSGalNAcT1*-null mice based on immunoblotting (Figure 1B) and RT–PCR (Figure 1C) analyses respectively. The *CSGalNAcT1*-null mice were viable and fertile. The protein and mRNA levels in heterozygous mice (*CSGalNAcT1*$^{+/-}$) were decreased to 38 % and 40 % respectively of those in the wild-type controls (Figures 1B and 1C). Other

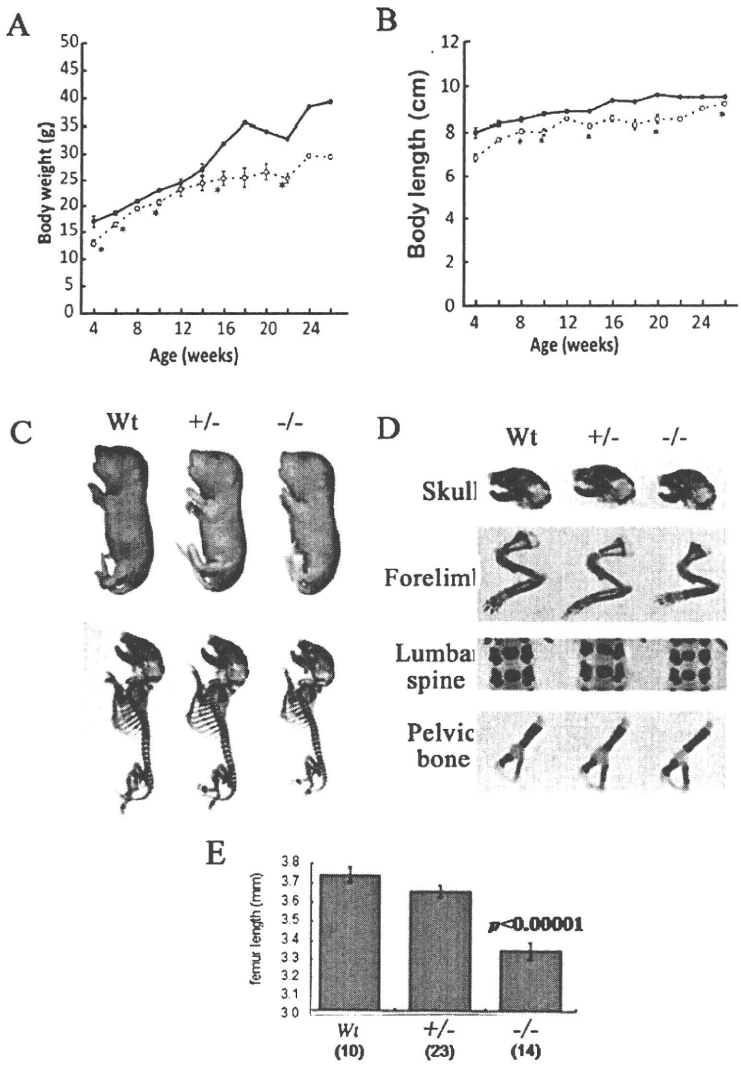

Figure 3 ***CSGalNAcT1*-null mice have reduced skeletal growth**

(**A** and **B**) The body weight (**A**) and the body length (**B**) in the wild-type (●) and *CSGalNAcT1*-null mice (○) during postnatal development. At 4 weeks after birth, the body mass and the body length of the null mice were slightly reduced compared with those of the wild-type.*$P < 0.05$ (Student's t test). (**C**) The fetal body (top panel) and skeleton (bottom panel) of wild-type (Wt), heterozygous (+/−) and null (−/−) mice. (**D**) Various bone segments of the fetal mice. Note that only forelimb bones of the null mice are shorter than those of wild-type mice. (**E**) Measurements of femur length. The femurs at E18.5 of the null mice are significantly shorter than those of wild-type and heterozygous mice (Student's t test, $P < 0.00001$). The number of the femurs measured for each genotype is shown in parentheses. The results are shown as means ± S.E.M.

enzymes related to CS synthesis, including CSGalNAcT2, a paralogue of CSGalNAcT1, were not up-regulated in the *CSGalNAcT1*-null mice (Figure 1C), indicating that no compensatory elevation in expression of related enzymes occurred.

The null mice were viable and fertile; however, we found a large number of abnormalities in the cartilages of these mice. CS production in the cartilage of heterozygous mice (64.4 ± 5.3 nmol/mg of protein) was not reduced compared with that of wild-type mice (63.0 ± 4.4 nmol/mg of protein); however, total CS content in *CSGalNAcT1*-null mice was less than half (31.0 ± 3.0 nmol/mg of protein; $n = 6$ of each; Figure 2A) of that in the wild-type controls. Normally, CS appears metachromatically violet in Toluidine Blue-stained samples. On the basis of Toluidine Blue staining, the cartilage of wild-type controls was enriched with CS, and the metachromasia indicative of CS was not observed in the *CSGalNAcT1*-null mice (Figure 2B). Consistent with observation of aggregated collagen fibres under electron microscopic observation, there were many speculate fibres in the *CSGalNAcT1*-null mice (see arrows in Figure 1B; also see below and Figure 5). CS in the null mice was compositionally similar to that in the control mice except for a reduction in the proportion of the non-sulfated disaccharide (Figure 2A).